
VOICEFIXER: TOWARD GENERAL SPEECH RESTORATION WITH NEURAL VOCODER

Haohe Liu^{1,2*}, Qiuqiang Kong¹, Qiao Tian¹, Yan Zhao¹,
DeLiang Wang², Chuanzeng Huang¹, Yuxuan Wang¹

¹ Speech, Audio and Music Intelligence (SAMI) group, ByteDance

² Department of Computer Science and Engineering, The Ohio State University

ABSTRACT

Speech restoration aims to remove distortions in speech signals. Prior methods mainly focus on *single-task speech restoration* (SSR), such as speech enhancement or speech declipping. However, SSR systems only focus on one task and do not address the general speech restoration problem. In addition, previous SSR systems show limited performance in some speech restoration tasks such as speech super-resolution. To overcome those limitations, we propose a *general speech restoration* (GSR) task that attempts to remove multiple distortions simultaneously. Furthermore, we propose *VoiceFixer*¹, a generative framework to address the GSR task. *VoiceFixer* consists of an *analysis stage* and a *synthesis stage* to mimic the speech analysis and comprehension of the human auditory system. We employ a ResUNet to model the analysis module and a neural vocoder to model the synthesis module. We evaluate *VoiceFixer* with additive noise, room reverberation, low-resolution, and clipping distortions. Our baseline GSR model achieves a 0.499 higher mean opinion score (MOS) than the speech enhancement SSR model. *VoiceFixer* further surpasses the GSR baseline model on MOS score by 0.256. Moreover, we observe that *VoiceFixer* generalizes well to severely degraded real speech recordings, indicating its potential in restoring old movies and historical speeches. The source code is available at https://github.com/haoheliu/voicefixer_main.

1 INTRODUCTION

Speech restoration is a process to restore degraded speech signals to high-quality speech signals. Speech restoration is an important research topic due to speech distortions are ubiquitous. For example, speech is usually surrounded by background noise, blurred by room reverberations, or recorded by low-quality devices (Godsill et al., 2002). Those distortions degrade the perceptual quality of speech for human listeners. Speech restoration has a wide range of applications such as online meeting (Defossez et al., 2020), hearing aids (Van den Bogaert et al., 2009), and audio editing (Van Winkle, 2008). Still, speech restoration remains a challenging problem due to the large variety of distortions in the world.

Previous works in speech restoration mainly focus on *single task speech restoration* (SSR), which deals with only one type of distortion at a time. For example, speech denoising (also known as speech enhancement) (Loizou, 2007), speech dereverberation (Naylor & Gaubitch, 2010), speech super-resolution (Kuleshov et al., 2017), or speech declipping (Záviška et al., 2020). However, in the real world, speech signal can be degraded by several different distortions simultaneously, which means previous SSR systems oversimplify the speech distortion types (Kashani et al., 2019; Lin

*Work done while interning at ByteDance.

¹Restoration samples can be found in <https://haoheliu.github.io/demopage-voicefixer>

et al., 2021; Kuleshov et al., 2017; Birnbaum et al., 2019). The mismatch between the training data used in SSR and the testing data from the real world degrades the speech restoration performance. Furthermore, previous methods typically apply one-stage systems to map from degraded speech to high-quality speech. However, those one-stage systems do not perform well on generative tasks such as speech super-resolution (Sulun & Davies, 2020; Kuleshov et al., 2017; Lin et al., 2021; Lee & Han, 2021).

To address the mismatch problem, we propose a new task called general speech restoration (GSR), which aims at restoring multiple distortions in a single model. A numerous studies (Cutler et al., 2021; Cauchi et al., 2014; Han et al., 2015) have reported the benefits of jointly training multiple speech restoration tasks. Nevertheless, performing GSR using one-stage systems suffer from the problems in each SSR method. Based on these observations, we propose a two-stage system called *VoiceFixer*.

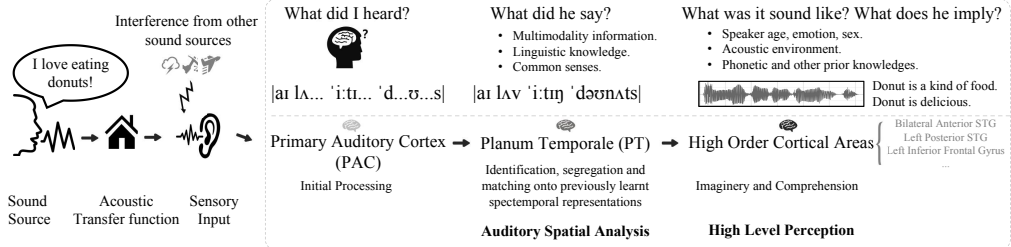


Figure 1: The neural and cognitive model of how human brain understand and restore distorted speech.

The design of *VoiceFixer* is motivated by the biological mechanisms of human hearing when restoring distorted speech (Kennedy-Higgins, 2019). Intuitively, if a person tries to identify a strongly distorted voice, his/her brain can recover the degraded speech by utilizing both the distorted speech signal and prior knowledge of the language. As shown in Figure 1, the distortion speech perception is modeled by neuroscientists as a two-stage process, including an *auditory scene analysis* stage (Bregman, 1994), and a *high level comprehension/synthesis* stage (Griffiths & Warren, 2002). In the analysis stage, the sound information is first transformed into acoustic features by primary auditory cortex (PAC). Then planum temporale (PT), the cortical area posterior to the auditory cortex, acts as a computational hub by segregating and matching the acoustic features to a low level spectrotemporal representations. In the synthesis stage, a high order cortical area is hypothesized to perform the high level perception tasks (Griffiths & Warren, 2002; Kennedy-Higgins, 2019). Our proposed *VoiceFixer* systems model the analysis stage with spectral transformations and a deep residual UNet, and the synthesis stage with a convolutional vocoder trained using adversarial losses. One advantage of the two-stage *VoiceFixer* is that the analysis and synthesis stages can be trained separately. Two-stage methods have also been successfully applied to the speech synthesis task (Wang et al., 2016; Ren et al., 2019; Lin et al., 2021) where acoustic models and vocoders are trained separately.

VoiceFixer is the first GSR model that is able to restore a wide range of low-resolution speech sampled from 2 kHz to 44.1 kHz, which is different from previous studies working on constant sampling rates (Lim et al., 2018; Wang & Wang, 2021; Lee & Han, 2021). To the best of our knowledge, *VoiceFixer* is the first model that jointly performs speech denoising, speech dereverberation, speech super-resolution, and speech declipping in a unified model.

The rest of this paper is organized as follows. Section 2 introduces the formulations of speech distortions. Section 3 describes the design of *VoiceFixer*. Section 5 discusses the evaluation results. Section 6 concludes this work and discusses future directions. Appendixes introduce related works and show speech restoration demos.

2 PROBLEM FORMULATION

We denote a segment of a speech signal as $s \in \mathbb{R}^L$, where L is the samples number in the segment. We model the distortion process of the speech signal as a function $d(\cdot)$. The degraded speech $x \in \mathbb{R}^L$

can be written as:

$$\mathbf{x} = d(\mathbf{s}). \quad (1)$$

Speech restoration is a task to restore high-quality speech $\hat{\mathbf{s}}$ from \mathbf{x} :

$$\hat{\mathbf{s}} = f(\mathbf{x}) \quad (2)$$

where $f(\cdot)$ is the restoration function and can be viewed as a reverse process of $d(\cdot)$. The target is to restore $\hat{\mathbf{s}}$ from the observed speech \mathbf{x} so that $\hat{\mathbf{s}}$ is as close to \mathbf{s} as possible. Recently, several deep learning based one-stage methods have been proposed to model $f(\cdot)$ such as fully connected neural networks, recurrent neural networks, and convolutional neural networks. More detailed introduction can be found in Appendix A.2.

Distortion modeling is an important step to simulate distorted speech when build speech restoration systems. Several previous works model distortions in a sequential order (Vincent et al., 2017; Cauchi et al., 2014; Tan et al., 2020; Zhao et al., 2019). Similarly, we model the distortion $d(\cdot)$ as a composite function:

$$d(\mathbf{x}) = d_1 \circ d_2 \circ \dots \circ d_Q(\mathbf{x}), d_q \in D, q = 1, 2, \dots, Q, \quad (3)$$

where \circ stands for function composition and Q is the number of distortions to consist $d(\cdot)$. Set $D = \{d_v(\cdot)\}_{v=1}^V$ is the set of distortion types where V is the total number of types. Equation 3 describes the procedure of compounding different distortions from D in a sequential order. We introduce four speech distortions as follows.

Additive noise is one of the most common distortion and can be modeled by the addition between speech \mathbf{s} and noise $\mathbf{n} \in \mathbb{R}^L$:

$$d_{\text{noise}}(\mathbf{s}) = \mathbf{s} + \mathbf{n}. \quad (4)$$

Reverberation is caused by the reflections of signal in a room. Reverberation makes speech signals sound distant and blurred. It can be modeled by convolving speech signals with room impulse response filter (RIR) \mathbf{r} :

$$d_{\text{rev}}(\mathbf{s}) = \mathbf{s} * \mathbf{r} \quad (5)$$

where $*$ stands for a convolution operation.

Low-resolution distortions refer to audio recordings that are recorded in low sampling rates or with limited bandwidth. There are many causes for low-resolution distortions, for example, microphones have low responses in the high frequency, or audio recordings are compressed to low sampling rates. We follow the description in Wang & Wang (2021) to produce low-resolution distortions but add more diverse filter types (Sulun & Davies, 2020). We first convolve \mathbf{s} with a low pass filter \mathbf{h} with random filter type to avoid the aliasing phenomenon. Then we perform resampling on the filtered result from the original sampling rate o to a lower sampling rate u .

$$d_{\text{low.res}}(\mathbf{s}) = \text{Resample}(\mathbf{s} * \mathbf{h}, o, u), \quad (6)$$

Clipping distortions refer to the clipped amplitude of audio signals, which are usually caused by low-quality microphones. Clipping can be modeled by restricting signal amplitudes within $[-\eta, +\eta]$:

$$d_{\text{clip}}(\mathbf{s}) = \max(\min(\mathbf{s}, \eta), -\eta), \eta \in [0, 1]. \quad (7)$$

In the frequency domain, clipping effect produces strong harmonic components in high frequencies and degrades speech intelligibility accordingly.

3 METHODOLOGY

3.1 ONE-STAGE SPEECH RESTORATION MODELS

Previous deep learning based speech restoration models are usually in one stage. That is, a model predicts restored speech $\hat{\mathbf{s}}$ from input \mathbf{x} directly:

$$f : \mathbf{x} \rightarrow \hat{\mathbf{s}}. \quad (8)$$

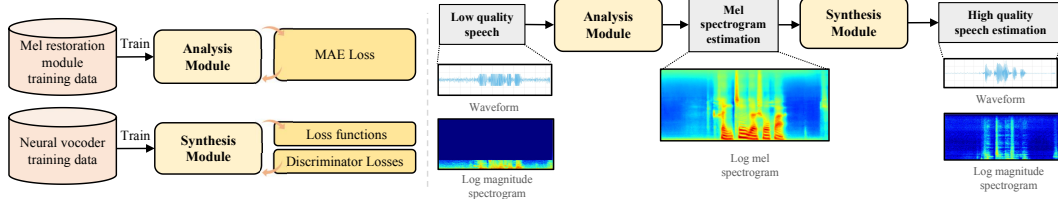


Figure 2: Overview of the proposed *VoiceFixer* system.

The mapping function $f(\cdot)$ can be modeled by time domain speech restoration systems such as one-dimensional convolutional neural networks (Luo & Mesgarani, 2019) or frequency domain systems such as mask-based (Narayanan & Wang, 2013) methods:

$$\hat{S} = (F_{\text{sp}}(|X|; \theta) \odot |X|) e^{j\angle X}. \quad (9)$$

where X is the short-time fourier transform (STFT) of x . X has a shape of $T \times F$ where T is the number of frame and F is the number of frequency bins. The output of the mask estimation function $F(\cdot; \theta)$ is multiplied by the magnitude spectrogram $|X|$ to produce the target spectrogram estimation \hat{S} . Then, inverse short-time fourier transform (iSTFT) is applied on \hat{S} to obtain \hat{s} . The one-stage speech restoration models are typically optimized by minimizing the mean absolute error (MAE) loss between the estimated spectrogram \hat{S} and the target spectrogram S :

$$\mathcal{L} = \left\| |\hat{S}| - |S| \right\|_1 \quad (10)$$

Previous one-stage models usually build on high-dimensional features such as time samples and the STFT spectrograms. However, Kuo & Sloan (2005); Trunk (1979) point out that the high-dimensional features will lead to exponential growth in search space. The model can take effect on the high-dimensional features under the premise of enlarging the model capacity but may also fail in challenging tasks. Therefore, it would be beneficial if we could build a system on more delicate low-dimensional features.

4 VOICEFIXER

In this study, we propose *VoiceFixer*, a two-stage speech restoration framework. Multi-stage methods have achieved state-of-the-art performance in many speech processing tasks (Jarrett et al., 2009; Takahama et al., 2019; Zhao et al., 2019; Tan et al., 2020). In speech restoration, our proposed *VoiceFixer* breaks the conventional one-stage system into a two-stage system:

$$f : x \mapsto z, \quad (11)$$

$$g : z \mapsto \hat{s}. \quad (12)$$

Equation 11 denotes the analysis stage of *VoiceFixer* where a distorted speech x is mapped into a representation z . Equation 12 denotes the synthesis stage of *VoiceFixer*, which synthesize z to the restored speech \hat{s} . Through the two-stage processing, *VoiceFixer* mimics the human perception of speech described in Section 1.

4.1 ANALYSIS STAGE

The goal of the analysis stage is to predict the intermediate representation z , which can be used later to recover the restored speech signals. In our study, we choose mel spectrogram as the intermediate representation. Mel spectrogram has been widely used in many speech proceessing tasks (Shen et al., 2018; Ren et al., 2019; Kong et al., 2019; Narayanan & Wang, 2013). The frequency dimension of mel spectrogram is usually much smaller than that of STFT thus can be regarded as a way of feature dimension reduction. So, the objective of the analysis stage becomes to restore mel spectrograms of the target signals. The mel spectrogram restoration process can be written as the following equation,

$$\hat{S}_{\text{mel}} = f_{\text{mel}}(X_{\text{mel}}; \alpha) \odot X_{\text{mel}}, \quad (13)$$

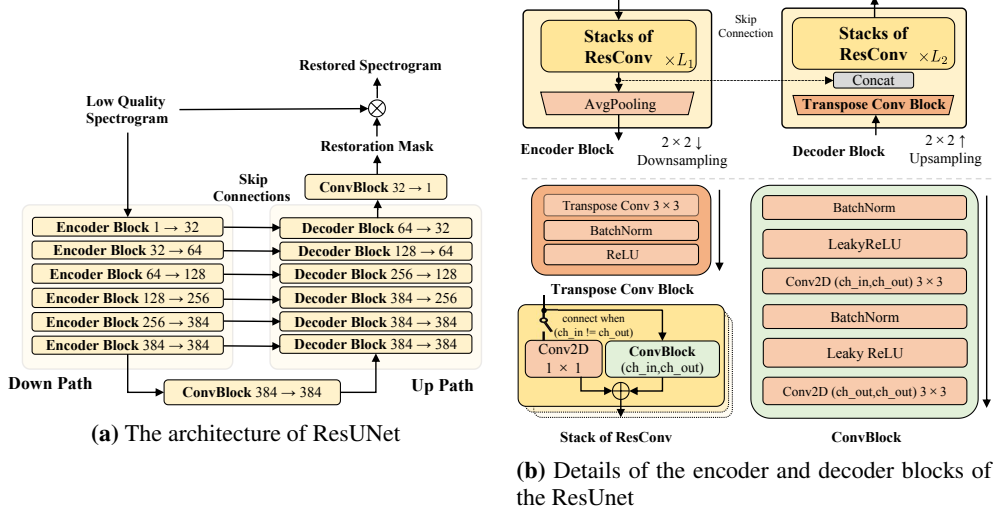


Figure 3: The architecture of ResUnet, which output have the same size as input.

where \mathbf{X}_{mel} is the mel spectrogram of \mathbf{x} . It is calculated by $\mathbf{X}_{\text{mel}} = \mathbf{X}\mathbf{W}$ where \mathbf{W} is a set of mel filter banks with shape of $F \times F'$. The mapping function $f_{\text{mel}}(\cdot; \alpha)$ is the mel restoration mask estimation module parameterized by α . The output of f_{mel} is multiplied by \mathbf{X}_{mel} to predict the target mel spectrogram.

We use ResUNet (Kong et al., 2021a) to model the analysis stage as shown in Figure 3a, which is an improved UNet (Ronneberger et al., 2015). The ResUNet consists of several encoder and decoder blocks. There are skip connections between encoder and decoder blocks at the same level. Figure 3b shows the details of the encoder and decoder block. Both encoder and decoder block share the same structure, which is a series of residual convolutions (ResConv). Each convolutional layer in ResConv consists of a batch normalization (BN) (Ioffe & Szegedy, 2015), a leaky ReLU activation (Xu et al., 2015), and a linear convolutional operation. The encoder blocks apply average pooling for down-sampling. The decoder blocks apply transpose convolution for up-sampling. In addition to ResUNet, we implement the analysis stage with fully connected deep neural network (DNN) (Ciregan et al., 2012; Szegedy et al., 2013), and bidirectional gated recurrent units (BiGRU) (Chung et al., 2014) for comparison. The DNN consists of six fully connected layers. The BiGRU have similar structures with DNN except for replacing the last two layers in DNN to bi-directional GRU layers.

The details of these three models are discussed in Appendix B.1. We will refer to *ResUNet* as *UNet* later for abbreviation. We optimize the analysis module using the MAE loss between the estimated mel spectrogram $\hat{\mathbf{S}}_{\text{mel}}$ and the target mel spectrogram \mathbf{S}_{mel} :

$$\mathcal{L}_{\text{ana}} = \left\| \hat{\mathbf{S}}_{\text{mel}} - \mathbf{S}_{\text{mel}} \right\|_1 \quad (14)$$

4.2 SYNTHESIS MODULE

The synthesis module is a neural vocoder that synthesizes the mel spectrogram into waveform as denoted in Equation 15.

$$\hat{\mathbf{s}} = g(\hat{\mathbf{X}}_{\text{mel}}; \beta), \quad (15)$$

where $g(\cdot; \beta)$ stands for the vocoder model parameterized by β . We employ a recently proposed non-autoregressive model time and frequency domain based generative adversarial network (TFGAN) as the vocoder.

Figure 4 shows the detailed architecture of TFGAN, in which the input mel spectrogram $\hat{\mathbf{X}}_{\text{mel}}$ will first pass through a condition network *CondNet*, which contains N_1 one-dimensional convolution (Conv1d) layers with exponential linear unit activations (Clevert et al., 2015). Then, in *UpNet*, it is upsampled N_2 times with ratios of s_0, s_1, \dots , and s_{N_2-1} using *UpsampleBlock* and *ResStacks*.

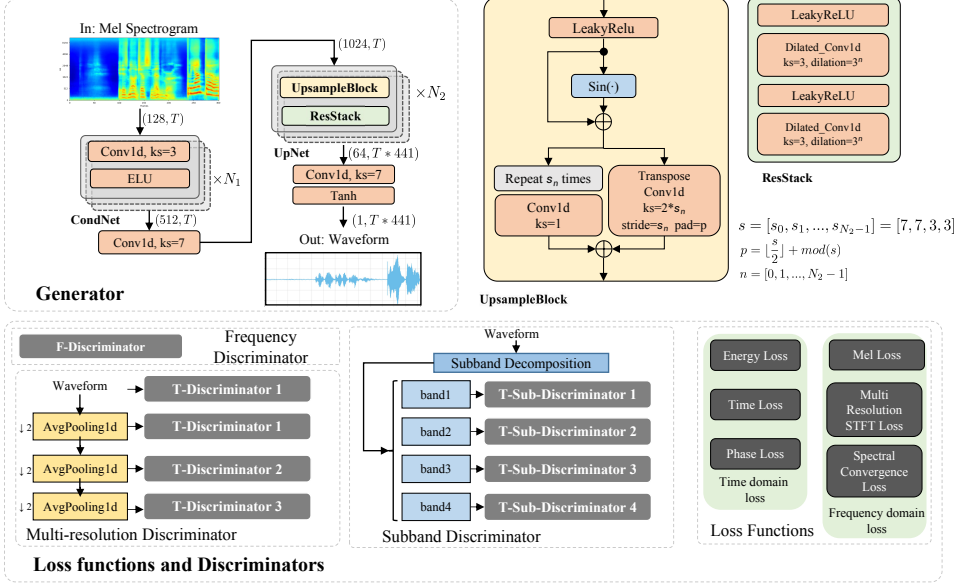


Figure 4: The architecture and training scheme of TFGAN, whose generator is later used as vocoder. The generator takes mel spectrogram as input and upsampled it into waveform. Both output waveform and its STFT spectrogram are used to compute loss. We employ both time and frequency discriminators for discriminative training.

Within the *UpsampleBlock*, the input is passed through a *LeakyReLU* activation and then fed into a sinusoidal function added to the original input to remove periodic artifacts in breathing part of speech. Then, the output is bifurcated into two branches for upsampling. One branch repeats the samples s_n times followed by a *Conv1d*. The other branch uses a stride s_n transpose convolution. The output of the repeat and transpose convolution branches are added together as the output of *UpsampleBlock*. *ResStacks* module contains two dilated convolution layers with *LeakyReLU* activations. The exponentially growing dilation in *ResStack* enable the model to capture long range dependencies. The TFGAN in our synthesis model applies $N_2 = 4$. After four *UpsampleBlock* blocks with ratios [7, 7, 3, 3], each frame of the mel spectrogram is transformed into a sequence with 441 samples corresponding to 10 ms of audio sampled at 44.1 kHz.

The training criteria of the synthesis module consists of frequency domain loss \mathcal{L}_F , time domain loss \mathcal{L}_T , and weighted discriminator loss \mathcal{L}_D :

$$\mathcal{L}_{\text{syn}} = \mathcal{L}_F + \mathcal{L}_T + \lambda_D \mathcal{L}_D, \quad (16)$$

The frequency domain loss \mathcal{L}_F is a combination of a mel loss \mathcal{L}_{mel} and multi-resolution STFT loss:

$$\mathcal{L}_F(\hat{s}, s) = \lambda_{\text{mel}} \mathcal{L}_{\text{mel}}(\hat{s}, s) + \sum_{k=1}^{K_F} (\lambda_{\text{sc}} \mathcal{L}_{\text{sc}}^{(k)}(\hat{s}, s) + \lambda_{\text{mag}} \mathcal{L}_{\text{mag}}^{(k)}(\hat{s}, s)) \quad (17)$$

where \mathcal{L}_{sc} and \mathcal{L}_{mag} are the spectrogram \mathcal{L}_1 loss calculated in the linear and log scale, respectively. There are K_F different window sizes ranging from 64 to 4096 to calculate \mathcal{L}_{sc} and \mathcal{L}_{mag} so that the trained vocoder is tolerant over phase mismatch (Yamamoto et al., 2020; Juvela et al., 2019; Wang et al., 2019). Table 2 in Appendix B.2 shows the detailed configurations.

Time domain loss is complementary to frequency domain loss to address artifacts such as periodic artifacts. Time domain loss combines segment loss $\mathcal{L}_{\text{seg}}^{(k)}$, energy loss $\mathcal{L}_{\text{energy}}^{(k)}$ and phase loss $\mathcal{L}_{\text{phase}}^{(k)}$:

$$\mathcal{L}_T(\hat{s}, s) = \sum_{k=1}^{K_T} (\lambda_{\text{energy}} \mathcal{L}_{\text{energy}}^{(k)}(\hat{s}, s) + \lambda_{\text{phase}} \mathcal{L}_{\text{phase}}^{(k)}(\hat{s}, s) + \lambda_{\text{seg}} \mathcal{L}_{\text{seg}}^{(k)}(\hat{s}, s)) \quad (18)$$

where segment loss $\mathcal{L}_{\text{seg}}^{(k)}$, energy loss $\mathcal{L}_{\text{energy}}^{(k)}$ and phase loss $\mathcal{L}_{\text{phase}}^{(k)}$ are described in Equation 24, 25, and 26 of Appendix B.2. There are K_T different window sizes ranging from 1 to 960 to calculate

time domain loss at different resolutions. The details of window sizes are shown in Table 3 of Appendix B.2. The energy loss and phase loss have the advantage of alleviating artificial sounds.

Discriminative training is an effective way to train neural vocoders (Kong et al., 2020; Kumar et al., 2019). In our study, we utilize a group of discriminators, including a multi-resolution time discriminator D_T , a subband discriminator D_{sub} , and frequency discriminator D_F :

$$D(\mathbf{s}) = D_{sub}(\mathbf{s}) + D_F(\mathbf{s}) + \sum_{r=1}^{R_T} D_T^{(r)}(\mathbf{s}) \quad (19)$$

$$\mathcal{L}_D(\mathbf{s}, \hat{\mathbf{s}}) = \min_g \max_D (\mathbb{E}_{\mathbf{s}}(\log(D(\mathbf{s}))) + \mathbb{E}_{\hat{\mathbf{s}}}(\log(1 - D(\hat{\mathbf{s}})))). \quad (20)$$

The multi-resolution discriminators D_T take signals from R_T kinds of time resolutions after average pooling as input. The subband discriminator D_{sub} performs subband decomposition (Liu et al., 2020) on the waveform, producing four subband signals to feed into four *T-discriminators*, respectively. Frequency discriminator D_F takes the linear spectrogram as input and outputs real or fake labels. The bottom part of Figure 4 shows the main idea of *T-discriminator* and *F-discriminator*. Appendix B.2 describes the detailed discriminator architectures.

There are two advantages of using neural vocoders in the synthesis stage. First, neural vocoders contain prior knowledge on the structural distribution of speech signals, which is important to restore distorted speech. Our vocoder is trained using a large amount of speech data with thousands of speakers, thus it can provide sufficient prior knowledge of speech signals. This amount of data is more than that used in conventional SSR methods with limited speakers. Second, the neural vocoders typically take the mel spectrogram as input, resulting in less feature dimensions than the STFT features. This helps to reduce computational cost and achieve better performance in analysis stage.

5 EXPERIMENTS

5.1 DATASETS AND EVALUATION METRICS

Training sets We use VCTK (Yamagishi et al., 2019) dataset to train the analysis module. AISHELL-3 (Shi et al., 2020), VCTK, and HQ-TTS (van Niekerk et al., 2017; Sodimana et al., 2018; Guevara-Rukoz et al., 2020) datasets are used to train the vocoder. We call the noise datasets used for training as VD-Noise. To simulate the reverberations, we employ a set of RIRs to create a RIR-44k dataset². The details of those datasets and the configures of RIRs are discussed in Appendix C.1.

Test sets³ We employ VCTK-Demand (Valentini-Botinhao et al., 2017) as the denoising test set and name it as DENOISE. We call our speech super-resolution, declipping, and dereverberation evaluation test sets as SR, DECLI, and DEREV, respectively. In addition, we create a ALL-GSR test set containing all distortions. We introduce the details of how we build these test sets in Appendix C.3.

Evaluation metrics The metrics we adopt include log-spectral distance (LSD) (Erell & Weintraub, 1990), wide band perceptual evaluation of speech quality (PESQ-wb) (Rix et al., 2001), structural similarity (SSIM) (Wang et al., 2004), and scale-invariant signal to noise ratio (SiSNR) (Le Roux et al., 2019). We use mean opinion scores (MOS) to subjectively evaluate different systems.

The output of vocoder is not strictly aligned on sample level with the target, as is often the case in generative model (Kumar et al., 2020). This effect will degrade the metrics, especially for those calculated on time samples such as SiSNR. So, to compensate SiSNR, we design a similar metrics, scale-invariant spectrogram to noise ratio (SiSPNR), to measure the discrepancies on spectrogram. Details of the metrics are described in Appendix C.4.

²<https://zenodo.org/record/5528124>

³<https://zenodo.org/record/5528144>

5.2 DISTORTION SIMULATION

For the SSR task, we perform only one type of distortion for evaluation. For the GSR task, we first assume that $D = \{d_{\text{noise}}, d_{\text{rev}}, d_{\text{low_res}}, d_{\text{clip}}\}$ because those distortions are the most common distortions in daily environment (Ribas et al., 2016). Second, we assume that $Q \leq 4$ in Equation 3. In other words, each distortion in D appears at most one time. Then, we generate the distortions with a specific order $d_{\text{low_res}}$, d_{rev} , d_{clip} , and d_{noise} . These distortions are added randomly using random configures.

5.3 BASELINE SYSTEMS

Table 5 in Appendix D summarizes all the experiments in this study. We implement several SSR and GSR systems using one-stage restoration models. For the GSR, we train a ResUNet model called *GSR-UNet* with all distortions. For the SSR model, we implement a *Denoise-UNet* for additive noise distortion, a *Dereverb-UNet* for reverberation distortion, a *SR-UNet* for low-resolution distortion, and a *Declip-UNet* for clipping distortion. For the SR task, we also include two state-of-the-art models, *NuWave* (Lee & Han, 2021) and *SEANet* (Li et al., 2021) for comparison. For Declipping, we compare with a state-of-the-art synthesis-based method *SSPADE* (Kitić et al., 2015; Záviška et al., 2019a) using the toolbox⁴ provided by Záviška et al. (2020). To explore the impact of model size of the mel restoration model, we setup ResUNets with two sizes. *UNet-S* and *UNet* have one and four *ResConv* blocks in each encoder and decoder block, respectively.

5.4 EVALUATION RESULTS

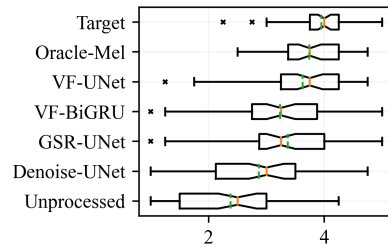
Neural vocoder To evaluate the performance of the neural vocoder, we compare with three baselines. The *Target* system denotes using the perfect s for evaluation. The *Unprocessed* system denotes using distorted speech x for evaluation. The *Oracle-Mel* system denotes using the mel spectrogram of perfect s as input to the vocoder. The *Oracle-Mel* system shows the performance of the vocoder. As shown in Table 1, the *Oracle-Mel* system achieves a MOS score of 3.74 which is close to the *Target* MOS of 3.95, indicating that the vocoder performs well in the synthesis task.

Models	PESQ	LSD	SiSPNR	SSIM	MOS
Unprocessed	1.94	2.00	7.20	0.64	2.38
Oracle-Mel	2.52	0.91	11.73	0.74	3.74
Target	4.64	0.01	110.55	1.00	3.95
GSR-UNet	2.67	1.01	12.19	0.79	3.37
Denoise-UNet	2.33	1.98	9.65	0.65	2.87
Dereverb-UNet	1.97	1.81	8.50	0.59	/
VF-DNN	1.55	1.18	10.13	0.68	/
VF-BiGRU	1.92	1.02	10.98	0.71	3.24
VF-UNet-S	2.01	1.02	11.09	0.71	/
VF-UNet	2.05	1.01	11.14	0.71	3.62

Table 1: Average PESQ, LSD, SiSPNR, SSIM and MOS scores on the general speech restoration test set ALL-GSR that includes all kinds of random distortions.

General speech restorations Table 1 shows the evaluation results of ALL-GSR test set. Figure 5 shows the box plot of the MOS scores of these systems. The *GSR-UNet* outperforms the two SSR models, *Denoise-UNet* and *Dereverb-UNet* by a large margin. It surpasses *Denoise-UNet* model by 0.5 on MOS score. This suggests GSR model is more powerful than SSR model on this test set. For convenience, we denote *VoiceFixer* as *VF* in tables and figures. We observe that the *VF-UNet* model achieves the highest MOS score and LSD score. Specifically, *VF-UNet* obtains 0.256 higher MOS score than that of *GSR-UNet*. This result indicates that *VoiceFixer* is better than ResUNet based one-stage model on overall quality. Also, we notice that the MOS score of *VF-UNet* is only 0.11 lower than the *Oracle-Mel*, demonstrating the good performance of the analysis module. The MOS score of *Oracle-Mel* is only 0.21 lower than *Target*, which means the signals processed by *Oracle-Mel* sound very close to the groundtruth. Among the *VoiceFixer* analysis models, the *UNet*

Figure 5: Box plot of the MOS scores on general speech restoration task. Red solid line and green dashed line represent median and mean value.



⁴<https://rajmic.github.io/declipping2020/>

front-end achieves the best. The *VF-BiGRU* model achieves similar subjective metrics with the *VF-UNet* model but has much lower MOS scores. This phenomenon shows that the improvement in subjective metrics in *VoiceFixer* is not always consistent with objective evaluation results.

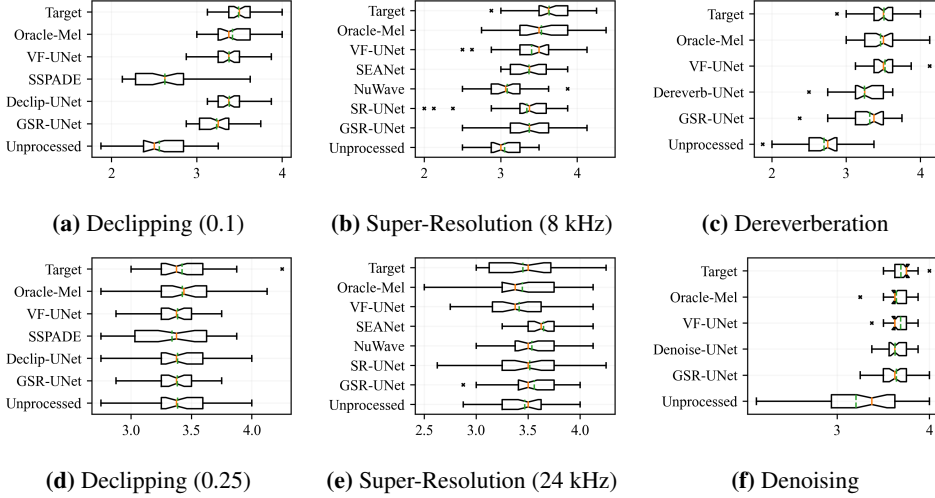


Figure 6: Box plot of the MOS scores on speech super-resolution, declipping, dereverberation and denoising.

Super-resolution Table 6 in Appendix D.1 shows the evaluation results on the super-resolution test set *SR*. For the 2 kHz, 4 kHz, and 8 kHz to 44.1 kHz super-resolution tasks, *VF-UNet* achieves a significantly higher LSD, SiSPNR and SSIM scores than other models. The LSD value of *VF-UNet* in 2 kHz sampling rate is still higher than the 8 kHz sampling rate score of *GSR-UNet*, *SR-UNet*, *NuWave*, and *SEANet*. This demonstrate the strong performance of *VoiceFixer* on dealing with low sampling rate cases. The *VF-BiGRU* model outperforms *VF-UNet-S* model on average scores for its better performance on low upsample-ratio cases. MOS box plot in Figure 6b shows that *VF-UNet* performs the best on 8 kHz to 44.1 kHz test set. Figure 6e shows the MOS score of *Unprocessed* is close to *Target* on 24 kHz to 44.1 kHz test set, meaning limited perceptual difference between the two sampling rate. On this test set, *SEANet* even achieves a higher MOS score than *Target*. That's due to its generated higher frequencies contain more energy comparing with groundtruth, making it sound more sparkle.

Denoising We evaluate the speech denoising performance on the *DENOISE* test set and show results in Table 7 in Appendix D.1. We find that *GSR-UNet* preserves more details in high-frequency part and has better PESQ and SiSPNR values than the denoising only SSR model *Denoise-UNet*. The reason might be that the data augmentation and joint performing super-resolution can increase the generalization and inpainting ability of the model (Hao et al., 2020). The PESQ score of *VF-UNet* reaches 2.43, higher than *SEGAN*, *WaveUNet*, and the model trained with weakly labeled data in Kong et al. (2021b). The MOS evaluation in Figure 6f on speech denoising task also demonstrates that the result of *VF-UNet* sound comparable with one-stage speech denoising models.

Declipping and dereverberation Table 9 and Table 8 in Appendix D.1 show similar performance trends on the speech declipping and speech dereverberation. In both tasks, the SSR model *Dereverb-UNet* and *Declip-UNet* achieve the highest scores. The performance of *GSR-UNet* is slightly worse, but it is acceptable considering that *GSR-UNet* does not need extra training for each task. *SSPADE* performs better on SiSNR but the PESQ and STOI scores are lower, especially in the 0.1 threshold case. The MOS score in Figure 6d shows that the clipping effect in the 0.25 threshold case is not easy to perceive, leading to high MOS score across all methods. In Figure 6a, both *Declip-UNet* and *VF-UNet* achieve the highest objective scores on the 0.1 threshold clipping test set. On dereverberation test set DEREV, *VF-UNet* achieves the highest MOS score 3.52.

6 CONCLUSION

In conclusion, *VoiceFixer* is an effective approach for speech restoration. It achieves a leading performance across all tasks. The evaluation results also show that models trained in a GSR way can perform comparably or even better than the SSR models.

REFERENCES

- Jacob Benesty, Shoji Makino, and Jingdong Chen. *Speech enhancement*. Springer Science & Business Media, 2006.
- Fanhui Bie, Dong Wang, Jun Wang, and Thomas Fang Zheng. Detection and reconstruction of clipped speech for speaker recognition. *Speech Communication*, pp. 218–231, 2015.
- Sawyer Birnbaum, Volodymyr Kuleshov, Zayd Enam, Pang Wei Koh, and Stefano Ermon. Temporal film: Capturing long-range sequence dependencies with feature-wise modulations. *arXiv preprint arXiv:1909.06628*, 2019.
- Albert S Bregman. *Auditory scene analysis: The perceptual organization of sound*. MIT press, 1994.
- Benjamin Cauchi, Ina Kodrasi, Robert Rehr, Stephan Gerlach, Ante Jukic, Timo Gerkmann, Simon Doclo, and Stefan Goetze. Joint dereverberation and noise reduction using beamforming and a single-channel speech enhancement scheme. In *Proc. REVERB Challenge Workshop*, pp. 1–8, 2014.
- Junyoung Chung, Caglar Gulcehre, KyungHyun Cho, and Yoshua Bengio. Empirical evaluation of gated recurrent neural networks on sequence modeling. *arXiv preprint arXiv:1412.3555*, 2014.
- Dan Ciregan, Ueli Meier, and Jürgen Schmidhuber. Multi-column deep neural networks for image classification. In *Proceedings of the IEEE/CVF Conference on Computer Vision and Pattern Recognition*, pp. 3642–3649, 2012.
- Djork-Arné Clevert, Thomas Unterthiner, and Sepp Hochreiter. Fast and accurate deep network learning by exponential linear units (elus). *arXiv preprint arXiv:1511.07289*, 2015.
- Ross Cutler, Ando Saabas, Tanel Parnamaa, Markus Loide, Sten Sootla, Marju Purin, Hannes Gamper, Sebastian Braun, Karsten Sorensen, Robert Aichner, et al. Acoustic echo cancellation challenge. In *INTERSPEECH*, 2021.
- Alexandre Defossez, Gabriel Synnaeve, and Yossi Adi. Real time speech enhancement in the waveform domain. *arXiv preprint arXiv:2006.12847*, 2020.
- Per Ekstrand. Bandwidth extension of audio signals by spectral band replication. In *Proceedings of the IEEE Benelux Workshop on Model Based Processing and Coding of Audio*. Citeseer, 2002.
- Adoram Erell and Mitch Weintraub. Estimation using log-spectral-distance criterion for noise-robust speech recognition. In *Proceedings of the IEEE Conference on Acoustics, Speech, and Signal Processing*, pp. 853–856, 1990.
- William Fong and Simon Godsill. Monte carlo smoothing for non-linearly distorted signals. In *Proceedings of the IEEE Conference on Acoustics, Speech, and Signal Processing*, pp. 3997–4000, 2001.
- Simon Godsill, Peter Rayner, and Olivier Cappé. Digital audio restoration. In *Applications of digital signal processing to audio and acoustics*, pp. 133–194. Springer, 2002.
- Timothy D Griffiths and Jason D Warren. The planum temporale as a computational hub. *Trends in neurosciences*, pp. 348–353, 2002.
- Adriana Guevara-Rukoz, Isin Demirsahin, Fei He, Shan-Hui Cathy Chu, Supheakmungkol Sarin, Knot Pipatsrisawat, Alexander Gutkin, Alena Butryna, and Oddur Kjartansson. Crowdsourcing Latin American Spanish for Low-Resource Text-to-Speech. In *Proceedings of The 12th Language Resources and Evaluation Conference*, pp. 6504–6513, Marseille, France, May 2020. European Language Resources Association. ISBN 979-10-95546-34-4. URL <https://www.aclweb.org/anthology/2020.lrec-1.801>.
- Archit Gupta, Brendan Shillingford, Yannis Assael, and Thomas C Walters. Speech bandwidth extension with wavenet. In *IEEE Workshop on Applications of Signal Processing to Audio and Acoustics*, pp. 205–208. IEEE, 2019.

- Kun Han, Yuxuan Wang, DeLiang Wang, William S Woods, Ivo Merks, and Tao Zhang. Learning spectral mapping for speech dereverberation and denoising. *IEEE/ACM Transactions on Audio, Speech, and Language Processing*, pp. 982–992, 2015.
- Peter SK Hansen. *Signal subspace methods for speech enhancement*. PhD thesis, Citeseer, 1997.
- Xiang Hao, Xiangdong Su, Shixue Wen, Zhiyu Wang, Yiqian Pan, Feilong Bao, and Wei Chen. Masking and inpainting: A two-stage speech enhancement approach for low snr and non-stationary noise. In *Proceedings of the IEEE Conference on Acoustics, Speech, and Signal Processing*, pp. 6959–6963, 2020.
- Yanxin Hu, Yun Liu, Shubo Lv, Mengtao Xing, Shimin Zhang, Yihui Fu, Jian Wu, Bihong Zhang, and Lei Xie. DCCRN: Deep complex convolution recurrent network for phase-aware speech enhancement. *arXiv preprint arXiv:2008.00264*, 2020.
- Sergey Ioffe and Christian Szegedy. Batch normalization: Accelerating deep network training by reducing internal covariate shift. In *International Conference on Machine Learning*, pp. 448–456. PMLR, 2015.
- Bernd Iser and Gerhard Schmidt. Neural networks versus codebooks in an application for bandwidth extension of speech signals. In *the 8th European Conference on Speech Communication and Technology*, 2003.
- Kevin Jarrett, Koray Kavukcuoglu, Marc’Aurelio Ranzato, and Yann LeCun. What is the best multi-stage architecture for object recognition? In *IEEE 12th International Conference on Computer Vision*, pp. 2146–2153. IEEE, 2009.
- Lauri Juvela, Bajibabu Bollepalli, Junichi Yamagishi, and Paavo Alku. GELP: GAN-Excited linear prediction for speech synthesis from mel-spectrogram. *arXiv preprint arXiv:1904.03976*, 2019.
- Thomas Kailath. Lectures on Wiener and Kalman filtering. In *Lectures on Wiener and Kalman Filtering*, pp. 1–143. Springer, 1981.
- Hamidreza Baradaran Kashani, Ata Jodeiri, Mohammad Mohsen Goodarzi, and Shabnam Gholam-dokht Firooz. Image to image translation based on convolutional neural network approach for speech declipping. *arXiv preprint arXiv:1910.12116*, 2019.
- Hideki Kawahara. Straight, exploitation of the other aspect of vocoder: Perceptually isomorphic decomposition of speech sounds. *Acoustical Science and Technology*, pp. 349–353, 2006.
- Dan Kennedy-Higgins. *Neural and cognitive mechanisms affecting perceptual adaptation to distorted speech*. PhD thesis, University College London, 2019.
- Keisuke Kinoshita, Marc Delcroix, Takuya Yoshioka, Tomohiro Nakatani, Emanuel Habets, Reinhold Haeb-Umbach, Volker Leutnant, Armin Sehr, Walter Kellermann, and Roland Maas. The REVERB challenge: A common evaluation framework for dereverberation and recognition of reverberant speech. In *IEEE Workshop on Applications of Signal Processing to Audio and Acoustics*, pp. 1–4. IEEE, 2013.
- Sran Kitić, Nancy Bertin, and Rémi Gribonval. Sparsity and cosparsity for audio declipping: a flexible non-convex approach. In *International Conference on Latent Variable Analysis and Signal Separation*, pp. 243–250. Springer, 2015.
- Jungil Kong, Jaehyeon Kim, and Jaekyoung Bae. HiFi-GAN: Generative adversarial networks for efficient and high fidelity speech synthesis. *arXiv preprint arXiv:2010.05646*, 2020.
- Qiuqiang Kong, Yong Xu, Iwona Sobieraj, Wenwu Wang, and Mark D Plumbley. Sound event detection and time-frequency segmentation from weakly labelled data. *IEEE/ACM Transactions on Audio, Speech, and Language Processing*, pp. 777–787, 2019.
- Qiuqiang Kong, Yin Cao, Haohe Liu, Keunwoo Choi, and Yuxuan Wang. Decoupling magnitude and phase estimation with deep resnet for music source separation. In *The International Society for Music Information Retrieval*, 2021a.

- Qiuqiang Kong, Haohe Liu, Xingjian Du, Li Chen, Rui Xia, and Yuxuan Wang. Speech enhancement with weakly labelled data from audioset. *arXiv preprint arXiv:2102.09971*, 2021b.
- Juho Kontio, Laura Laaksonen, and Paavo Alku. Neural network-based artificial bandwidth expansion of speech. *IEEE/ACM Transactions on Audio, Speech, and Language Processing*, pp. 873–881, 2007.
- Volodymyr Kuleshov, S Zayd Enam, and Stefano Ermon. Audio super resolution using neural networks. *arXiv preprint arXiv:1708.00853*, 2017.
- Kundan Kumar, Rithesh Kumar, Thibault de Boissiere, Lucas Gestin, Wei Zhen Teoh, Jose Sotelo, Alexandre de Brébisson, Yoshua Bengio, and Aaron Courville. Melgan: Generative adversarial networks for conditional waveform synthesis. *arXiv preprint arXiv:1910.06711*, 2019.
- Rithesh Kumar, Kundan Kumar, Vicki Anand, Yoshua Bengio, and Aaron Courville. NU-GAN: High resolution neural upsampling with gan. *arXiv preprint arXiv:2010.11362*, 2020.
- Frances Y Kuo and Ian H Sloan. Lifting the curse of dimensionality. *Notices of the American Mathematical Society*, pp. 1320–1328, 2005.
- Jonathan Le Roux, Scott Wisdom, Hakan Erdogan, and John R Hershey. SDR–half-baked or well done? In *Proceedings of the IEEE Conference on Acoustics, Speech, and Signal Processing*, pp. 626–630, 2019.
- Katia Lebart, Jean-Marc Boucher, and Philip N Denbigh. A new method based on spectral subtraction for speech dereverberation. *Acta Acustica united with Acustica*, pp. 359–366, 2001.
- Junhyeok Lee and Seungu Han. Nu-wave: A diffusion probabilistic model for neural audio upsampling. *arXiv preprint arXiv:2104.02321*, 2021.
- Kehuang Li and Chin-Hui Lee. A deep neural network approach to speech bandwidth expansion. In *Proceedings of the IEEE Conference on Acoustics, Speech, and Signal Processing*, pp. 4395–4399, 2015.
- Yunpeng Li, Marco Tagliasacchi, Oleg Rybakov, Victor Ungureanu, and Dominik Roblek. Real-time speech frequency bandwidth extension. In *Proceedings of the IEEE Conference on Acoustics, Speech, and Signal Processing*, pp. 691–695, 2021.
- Teck Yian Lim, Raymond A Yeh, Yijia Xu, Minh N Do, and Mark Hasegawa-Johnson. Time-frequency networks for audio super-resolution. In *Proceedings of the IEEE Conference on Acoustics, Speech, and Signal Processing*, pp. 646–650, 2018.
- Ju Lin, Yun Wang, Kaustubh Kalgaonkar, Gil Keren, Didi Zhang, and Christian Fuegen. A two-stage approach to speech bandwidth extension. *INTERSPEECH*, pp. 1689–1693, 2021.
- Haohe Liu, Lei Xie, Jian Wu, and Geng Yang. Channel-wise subband input for better voice and accompaniment separation on high resolution music. *arXiv preprint arXiv:2008.05216*, 2020.
- QG Liu, B Champagne, and KC Ho. On the use of a modified fast affine projection algorithm in subbands for acoustic echo cancelation. In *IEEE Digital Signal Processing Workshop Proceedings*, pp. 354–357. IEEE, 1996.
- Philipos C Loizou. *Speech enhancement: theory and practice*. CRC press, 2007.
- Yi Luo and Nima Mesgarani. Conv-tasnet: Surpassing ideal time–frequency magnitude masking for speech separation. *IEEE Transactions on Acoustics, Speech, and Signal Processing*, pp. 1256–1266, 2019.
- Wolfgang Mack and Emanuël AP Habets. Declipping speech using deep filtering. In *IEEE Workshop on Applications of Signal Processing to Audio and Acoustics*, pp. 200–204. IEEE, 2019.
- Rainer Martin. Spectral subtraction based on minimum statistics. *Power*, 1994.
- Annamaria Mesaros, Toni Heittola, and Tuomas Virtanen. A multi-device dataset for urban acoustic scene classification. *arXiv preprint arXiv:1807.09840*, 2018.

- Masanori Morise, Fumiya Yokomori, and Kenji Ozawa. World: a vocoder-based high-quality speech synthesis system for real-time applications. *IEICE Transactions on Information and Systems*, pp. 1877–1884, 2016.
- Anna K Nábělek, Tomasz R Letowski, and Frances M Tucker. Reverberant overlap-and self-masking in consonant identification. *The Journal of the Acoustical Society of America*, pp. 1259–1265, 1989.
- Yoshihisa Nakatoh, Mineo Tsushima, and Takeshi Norimatsu. Generation of broadband speech from narrowband speech based on linear mapping. *Electronics and Communications in Japan (Part II: Electronics)*, pp. 44–53, 2002.
- Arun Narayanan and DeLiang Wang. Ideal ratio mask estimation using deep neural networks for robust speech recognition. In *Proceedings of the IEEE Conference on Acoustics, Speech, and Signal Processing*, pp. 7092–7096, 2013.
- Patrick A Naylor and Nikolay D Gaubitch. *Speech dereverberation*. Springer Science & Business Media, 2010.
- Aaron van den Oord, Sander Dieleman, Heiga Zen, Karen Simonyan, Oriol Vinyals, Alex Graves, Nal Kalchbrenner, Andrew Senior, and Koray Kavukcuoglu. Wavenet: A generative model for raw audio. *arXiv preprint arXiv:1609.03499*, 2016.
- Santiago Pascual, Antonio Bonafonte, and Joan Serra. SEGAN: Speech enhancement generative adversarial network. *arXiv preprint arXiv:1703.09452*, 2017.
- Wei Ping, Kainan Peng, Kexin Zhao, and Zhao Song. Waveflow: A compact flow-based model for raw audio. In *International Conference on Machine Learning*, pp. 7706–7716. PMLR, 2020.
- Adam Polyak, Lior Wolf, Yossi Adi, Ori Kabeli, and Yaniv Taigman. High fidelity speech regeneration with application to speech enhancement. In *Proceedings of the IEEE Conference on Acoustics, Speech, and Signal Processing*, pp. 7143–7147, 2021.
- Ryan Prenger, Rafael Valle, and Bryan Catanzaro. Waveglow: A flow-based generative network for speech synthesis. In *Proceedings of the IEEE Conference on Acoustics, Speech, and Signal Processing*, pp. 3617–3621, 2019.
- Joko Radic and Nikola Rozic. Reconstruction of the samples corrupted with impulse noise in multi-carrier systems. In *IEEE Wireless Communications and Networking Conference*, pp. 1–5. IEEE, 2009.
- Yi Ren, Yangjun Ruan, Xu Tan, Tao Qin, Sheng Zhao, Zhou Zhao, and Tie-Yan Liu. FastSpeech: Fast, robust and controllable text to speech. *arXiv preprint arXiv:1905.09263*, 2019.
- Lucas Rencker, Francis Bach, Wenwu Wang, and Mark D Plumley. Sparse recovery and dictionary learning from nonlinear compressive measurements. *IEEE Transactions on Signal Processing*, pp. 5659–5670, 2019.
- Dayana Ribas, Emmanuel Vincent, and José Ramón Calvo. A study of speech distortion conditions in real scenarios for speech processing applications. In *2016 IEEE Spoken Language Technology Workshop (SLT)*, pp. 13–20. IEEE, 2016.
- Antony W Rix, John G Beerends, Michael P Hollier, and Andries P Hekstra. Perceptual evaluation of speech quality (pesq)-a new method for speech quality assessment of telephone networks and codecs. In *Proceedings of the IEEE Conference on Acoustics, Speech, and Signal Processing*, pp. 749–752, 2001.
- Olaf Ronneberger, Philipp Fischer, and Thomas Brox. U-net: Convolutional networks for biomedical image segmentation. In *International Conference on Medical image computing and computer-assisted intervention*, pp. 234–241. Springer, 2015.
- Tara N Sainath, Oriol Vinyals, Andrew Senior, and Haşim Sak. Convolutional, long short-term memory, fully connected deep neural networks. In *Proceedings of the IEEE Conference on Acoustics, Speech, and Signal Processing*, pp. 4580–4584, 2015.

- Boaz Schwartz, Sharon Gannot, and Emanuël AP Habets. Online speech dereverberation using kalman filter and em algorithm. *IEEE/ACM Transactions on Audio, Speech, and Language Processing*, pp. 394–406, 2014.
- Jonathan Shen, Ruoming Pang, Ron J Weiss, Mike Schuster, Navdeep Jaitly, Zongheng Yang, Zhifeng Chen, Yu Zhang, Yuxuan Wang, Rj Skerrv-Ryan, et al. Natural TTS synthesis by conditioning wavenet on Mel spectrogram predictions. In *Proceedings of the IEEE Conference on Acoustics, Speech, and Signal Processing*, pp. 4779–4783, 2018.
- Yao Shi, Hui Bu, Xin Xu, Shaoji Zhang, and Ming Li. Aishell-3: A multi-speaker mandarin tts corpus and the baselines. *arXiv preprint arXiv:2010.11567*, 2020.
- Xiaofeng Shu, Yehang Zhu, Yanjie Chen, Li Chen, Haohe Liu, Chuanzeng Huang, and Yuxuan Wang. Joint echo cancellation and noise suppression based on cascaded magnitude and complex mask estimation. *arXiv preprint arXiv:2107.09298*, 2021.
- Brett Y Smolenski and Ravi P Ramachandran. Usable speech processing: A filterless approach in the presence of interference. *IEEE Circuits and Systems Magazine*, pp. 8–22, 2011.
- Keshan Sodimana, Knot Pipatsrisawat, Linne Ha, Martin Jansche, Oddur Kjartansson, Pasindu De Silva, and Supheakmungkol Sarin. A Step-by-Step Process for Building TTS Voices Using Open Source Data and Framework for Bangla, Javanese, Khmer, Nepali, Sinhala, and Sundanese. In *Proc. The 6th Intl. Workshop on Spoken Language Technologies for Under-Resourced Languages*, pp. 66–70, Gurugram, India, August 2018. URL <http://dx.doi.org/10.21437/SLTU.2018-14>.
- Serkan Sulun and Matthew EP Davies. On filter generalization for music bandwidth extension using deep neural networks. *IEEE Journal of Selected Topics in Signal Processing*, pp. 132–142, 2020.
- Christian Szegedy, Alexander Toshev, and Dumitru Erhan. Deep neural networks for object detection. 2013.
- Shusuke Takahama, Yusuke Kurose, Yusuke Mukuta, Hiroyuki Abe, Masashi Fukayama, Akihiko Yoshizawa, Masanobu Kitagawa, and Tatsuya Harada. Multi-stage pathological image classification using semantic segmentation. In *Proceedings of the IEEE/CVF International Conference on Computer Vision*, pp. 10702–10711, 2019.
- Ke Tan, Yong Xu, Shi-Xiong Zhang, Meng Yu, and Dong Yu. Audio-visual speech separation and dereverberation with a two-stage multimodal network. *IEEE Journal of Selected Topics in Signal Processing*, pp. 542–553, 2020.
- Qiao Tian, Yi Chen, Zewang Zhang, Heng Lu, Linghui Chen, Lei Xie, and Shan Liu. TFGAN: Time and frequency domain based generative adversarial network for high-fidelity speech synthesis. *arXiv preprint arXiv:2011.12206*, 2020.
- Gerard V Trunk. A problem of dimensionality: A simple example. *IEEE Transactions on pattern analysis and machine intelligence*, (3):306–307, 1979.
- Cassia Valentini-Botinhao et al. Noisy speech database for training speech enhancement algorithms and TTS models. 2017.
- Jean-Marc Valin and Jan Skoglund. Lpcnet: Improving neural speech synthesis through linear prediction. In *Proceedings of the IEEE Conference on Acoustics, Speech, and Signal Processing*, pp. 5891–5895, 2019.
- Tim Van den Bogaert, Simon Doclo, Jan Wouters, and Marc Moonen. Speech enhancement with multichannel wiener filter techniques in multimicrophone binaural hearing aids. *The Journal of the Acoustical Society of America*, pp. 360–371, 2009.
- Daniel van Niekerk, Charl van Heerden, Marelief Davel, Neil Kleynhans, Oddur Kjartansson, Martin Jansche, and Linne Ha. Rapid development of TTS corpora for four South African languages. In *INTERSPEECH*, pp. 2178–2182, Stockholm, Sweden, 2017.

- Charles Van Winkle. Audio analysis and spectral restoration workflows using adobe audition. In *Audio Engineering Society Conference: 33rd International Conference: Audio Forensics-Theory and Practice*. Audio Engineering Society, 2008.
- Emmanuel Vincent, Shinji Watanabe, Aditya Arie Nugraha, Jon Barker, and Ricard Marixer. An analysis of environment, microphone and data simulation mismatches in robust speech recognition. *Computer Speech & Language*, pp. 535–557, 2017.
- Heming Wang and DeLiang Wang. Towards robust speech super-resolution. *IEEE/ACM Transactions on Audio, Speech, and Language Processing*, 2021.
- Hong Wang and Fumitada Itakura. Dereverberation of speech signals based on sub-band envelope estimation. *IEICE Transactions on Fundamentals of Electronics, Communications and Computer Sciences*, pp. 3576–3583, 1991.
- Wenfu Wang, Shuang Xu, and Bo Xu. First step towards end-to-end parametric tts synthesis: Generating spectral parameters with neural attention. In *INTERSPEECH*, pp. 2243–2247, 2016.
- Xin Wang, Shinji Takaki, and Junichi Yamagishi. Neural source-filter-based waveform model for statistical parametric speech synthesis. In *Proceedings of the IEEE Conference on Acoustics, Speech, and Signal Processing*, pp. 5916–5920, 2019.
- Zhou Wang, Alan C Bovik, Hamid R Sheikh, and Eero P Simoncelli. Image quality assessment: from error visibility to structural similarity. *IEEE Transactions on Image Processing*, pp. 600–612, 2004.
- Donald S Williamson and DeLiang Wang. Time-frequency masking in the complex domain for speech dereverberation and denoising. *IEEE/ACM Transactions on Audio, Speech, and Language Processing*, pp. 1492–1501, 2017.
- Bing Xu, Naiyan Wang, Tianqi Chen, and Mu Li. Empirical evaluation of rectified activations in convolutional network. *arXiv preprint arXiv:1505.00853*, 2015.
- Junichi Yamagishi, Christophe Veaux, Kirsten MacDonald, et al. Cstr vctk corpus: English multi-speaker corpus for cstr voice cloning toolkit (version 0.92). 2019.
- Ryuichi Yamamoto, Eunwoo Song, and Jae-Min Kim. Parallel WaveGAN: A fast waveform generation model based on generative adversarial networks with multi-resolution spectrogram. In *Proceedings of the IEEE Conference on Acoustics, Speech, and Signal Processing*, pp. 6199–6203, 2020.
- Chengzhu Yu, Heng Lu, Na Hu, Meng Yu, Chao Weng, Kun Xu, Peng Liu, Deyi Tuo, Shiyin Kang, Guangzhi Lei, et al. Durian: Duration informed attention network for multimodal synthesis. *arXiv preprint arXiv:1909.01700*, 2019.
- Pavel Záviška, Pavel Rajmic, Ondřej Mokrý, and Zdeněk Průša. A proper version of synthesis-based sparse audio declipper. In *Proceedings of the IEEE Conference on Acoustics, Speech, and Signal Processing*, pp. 591–595, 2019a.
- Pavel Záviška, Pavel Rajmic, and Jiří Schimmel. Psychoacoustically motivated audio declipping based on weighted L_1 minimization. In *2019 42nd International Conference on Telecommunications and Signal Processing*, pp. 338–342. IEEE, 2019b.
- Pavel Záviška, Pavel Rajmic, Alexey Ozerov, and Lucas Rencker. A survey and an extensive evaluation of popular audio declipping methods. *IEEE Journal of Selected Topics in Signal Processing*, pp. 5–24, 2020.
- Yan Zhao, Zhong-Qiu Wang, and DeLiang Wang. Two-stage deep learning for noisy-reverberant speech enhancement. *IEEE/ACM Transactions on Audio, Speech, and Language Processing*, pp. 53–62, 2019.

A APPENDIX A

A.1 SPEECH DISTORTIONS

For the distortion types, firstly, the noise signal \mathbf{n} from another sound source can interference with the original speech, degrading its intelligibility. To address this problem, Researchers proposed to conduct speech denoising (Benesty et al., 2006) to remove the undesired noise. Secondly, even in an absolutely quiet environment, speech can interference with itself because the signal microphone receives is not only the original speech, but also echos and reflections. These distortions can be handled with acoustic echo cancelation (AEC) (Liu et al., 1996), and speech dereverberation (Naylor & Gaubitch, 2010). Third, speech distortions caused by hardware deficiencies are also common. If a recording device has low response in the high-frequency part, its recording will result in a loss in the higher frequencies, making the speech sound less clear. In this case, band width extension (BWE) (Ekstrand, 2002) and audio super resolution (SR) (Kuleshov et al., 2017) can be used to predict the higher frequencies. Other methods like click and pop removal (Smolenski & Ramchandran, 2011), corrupted samples replacement (Radic & Rozic, 2009), and declipping (Fong & Godsill, 2001) are also common restoration algorithms for low quality recordings.

A.2 RELATED WORKS

A.2.1 SPEECH RESTORATION TASKS

Audio super-resolution A lot of early study (Nakatoh et al., 2002; Iser & Schmidt, 2003; Kontio et al., 2007) break SR into spectral envelop estimation and excitation generation from the low-resolution part. At that time, the direct mapping from the low-resolution part to the high-resolution feature is not widely explored since the dimension of the high-resolution part is relatively high. Later, deep neural network (Li & Lee, 2015; Kuleshov et al., 2017) is introduced to perform SR using spectral mapping. These approaches show better subjective quality comparing with traditional methods. Later, to increase the modeling capacity, *TFilm* (Birnbaum et al., 2019) is proposed to model the affine transformation among each time block. *WaveNet* also shows effectiveness in extending the bandwidth of a band-limited speech (Gupta et al., 2019). To utilize the information both from the time and frequency domain, (Wang & Wang, 2021) proposed a time-frequency loss that can yield a balanced performance both on time and frequency domain metrics. Recently, *NU-GAN* (Kumar et al., 2020) and *NU-Wave* (Lee & Han, 2021) pushed the target sample rate in SR to high fidelity, up to 44.1 kHz and 48 kHz.

Although employing deep neural network in BWE show promising results, the generalization capability of these methods are still limited. For example, previous approaches (Kuleshov et al., 2017; Gupta et al., 2019) usually train and test models with a fix setting, i.e., a fix initial sample rate and target sample rate. However, in real world applications, speech bandwidth is not usually constant. Also, since the high-low quality speech pair is impossible to collect, BWE model usually produce low quality audio with lowpass filter during training. In this case, system tend to suffer from overfitting on a specific kind of lowpass filter. As mentioned in (Sulun & Davies, 2020), when the kind of filter used during training and testing differ, the performance can fall considerably. To alleviate filter overfitting, (Sulun & Davies, 2020) proposed to train model with multiple kinds of lowpass filters. By performing data augmentation in this way, unseen filter can be handled properly.

Speech declipping The methods for speech declipping can be categorized as supervised methods and unsupervised methods. The unsupervised, or blind methods usually perform declipping based on some generic regularization and assumption of what natural audio should look like, such as AS-PADE (Kitić et al., 2015), Dictionary Learning (Rencker et al., 2019), and Psychoacoustically motivated 11 minimization (Záviška et al., 2019b). The supervised models, mostly based on DNN (Bie et al., 2015; Mack & Habets, 2019), are usually trained on clipped and target data pair. For example, Kashani et al. (2019) treat the declipping as an image-to-image translation problem and utilize the *UNet* to do the spectral mapping. Currently, most of the state-of-the-art methods are unsupervised (Záviška et al., 2020) because they are usually designed to work on all kinds of audio, while the supervised model mainly specialized on the type of their training data. However, Záviška et al. (2020) believes supervised model still have the potential for better declipping performance.

Speech denoising Many methods have been proposed in speech denoising. Classical methods are efficient and effective on stationary noise, such as spectral subtraction (Martin, 1994), wiener and kalman filtering (Kailath, 1981), and subspace methods (Hansen, 1997) By comparison, deep learning based model such as *CLDNN* (Sainath et al., 2015), *Conv-TasNet* (Luo & Mesgarani, 2019) show higher subjective score and robustness on complex cases. Recently, new schemes have emerged for the training of SE model. *SEGAN* (Pascual et al., 2017) tried a generative way to train denoising model. *DCCRN* (Hu et al., 2020) employ the full complex network to perform denoising. Kong et al. (2021b) achieved a denoising model using only weakly labeled data. And Polyak et al. (2021) realize a denoising model using a regeneration approach.

Speech dereverberation Some of the early methods in speech dereverberation, such as Inverse filtering (Naylor & Gaubitch, 2010) and sub-band envelope estimation (Wang & Itakura, 1991), aiming at deconvolve the reverberate signal by estimating an inverse filter. But actually, the inverse filter is hard and not robust to do the precise estimate. Other techniques, spectral subtraction (Lebart et al., 2001), is based on an important overlap-masking (Nábělek et al., 1989) effect of reverberation. Schwartz et al. (2014) perform dereverberation using kalman-filter and expectation maximization algorithm. Recently, deep learning based dereverberation methods have emerged as the state of the art. Han et al. (2015) use fully connected deep neural network (DNN) to learn a spectral mapping from reverberate speech to clean speech. In Williamson & Wang (2017), similar to the masking-based denoising methods, authors proposed to do time-frequency mask estimation to perform dereverberation.

A.2.2 JOINT RESTORATION AND SYNTHETIC RESTORATION

Joint restoration Many works have adopted the joint restoration to improve models. To make the Acoustic Echo Cancellation (AEC) result sound cleaner, *MC-TCN* (Shu et al., 2021) proposed to jointly perform AEC and noise suppression at the same time. *MC-TCN* achieved a mean opinion score of 4.41, outperforming the baseline of INTERSPEECH2021 AEC Challenge (Cutler et al., 2021) by 0.54. What’s more, in the REVERB challenge (Kinoshita et al., 2013), the test set has both reverberation and noise. So the methods (Cauchi et al., 2014) in this challenge need to both perform denoising and dereverberation. Later, in Han et al. (2015), the authors proposed to perform dereverberation and denoising within a single DNN and substantially outperform related methods regarding quality and intelligibility. However, previous joint processing usually involved only two sub-tasks, which are usually denoising and a main task. In our work, we tried to joint performing four or more tasks so that to achieve general restoration.

Synthetic Restoration Directly estimate the source signal from the input mixture is hard sometimes especially when the source signal to noise ratio (SNR) is low. Some works adopted a regeneration approach. In Polyak et al. (2021), the authors utilize an ASR model, a pitch extraction model, and a loudness model to extract semantic level information from the speaker. Then they used these features in an encode-decoder network to do the regeneration of speech. To maintain the consistency of speaker characteristics. It uses an auxiliary identity network to compute the identity feature. Besides the restoration task, Text-to-Speech (TTS), is another heated research area. Similar to synthetic speech restoration, which regenerates restored speech from distorted speech, TTS can be treated as the regeneration of speech from texts.

A.2.3 NEURAL VOCODER

Vocoder, which can map the encoded speech feature to the waveform, is an indispensable component in various speech synthesis tasks. The most widely used input feature for vocoder is mel spectrogram. In recent years, since the emergence of *WaveNet* (Oord et al., 2016), neural network based vocoder starts to demonstرات clear advantages over traditional parametric vocoders (Morise et al., 2016; Kawahara, 2006). Comparing with traditional methods, the quality of *WaveNet* is more closer to human voice. Later, *WaveRNN* (Yu et al., 2019) is proposed to model the waveform with a single GRU. In this way, *WaveRNN* has much lower complexity comparing with *WaveNet*. To improve the efficiency, *LPCNet* (Valin & Skoglund, 2019) combines linear prediction with RNN, which significantly improves inference speed. However, the autoregressive nature of these models and extremely deep structure make their inference process hard to speed up by parallelism. To address this problem, non-autoregressive models like *WaveGlow* (Prenger et al., 2019) and *WaveFlow* (Ping et al., 2020) are proposed. Afterward, non-autoregressive GAN based models such as Yamamoto et al. (2020);

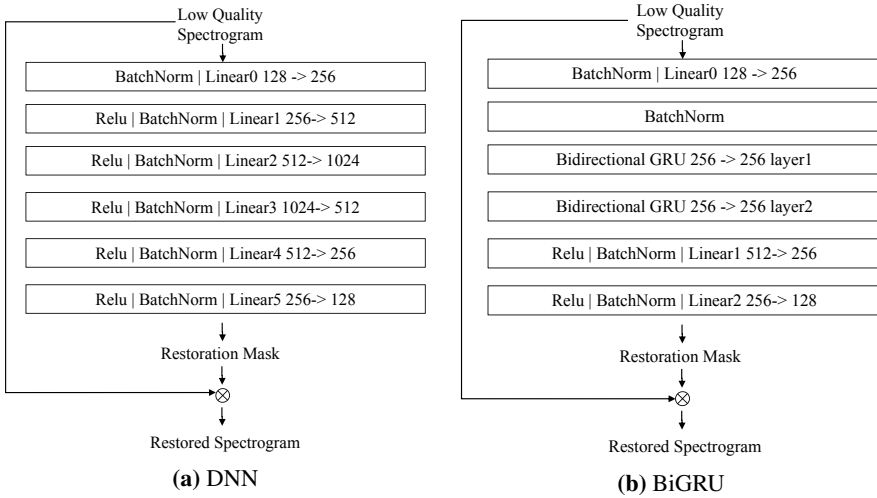


Figure 7: The architecture of DNN and Bi-RU we used

Kumar et al. (2019) push the synthesis quality to a comparable level with auto-regressive models. Recently, *TFGAN* (Tian et al., 2020) demonstrated strong capability in vocoding. Directed by frequency discriminator and multiple time-domain loss, *TFGAN* learns waveform information both in the time domain and frequency domain. As a result, the synthesis quality of *TFGAN* is more natural and less metallic comparing with other GAN-based non-auto-regressive models. In this work, we realize a universal vocoder based on *TFGAN*, which can reconstruct waveform from mel spectrogram with good perceptual quality. We open-source the pretrained vocoder for the convenience of later research and reproduction of this work.

B APPENDIX B

B.1 ANALYSIS MODULE ARCHITECTURE

The DNN and BiGRU we used are shown in Figure 7. the DNN we use in this module is a six layers fully connected network with BatchNorm and ReLU activations. The DNN accept each time step of the low-quality spectrogram as the input feature and output the restoration mask. Similarly, for the BiGRU model, we substitute some layers in DNN to a two-layer bidirectional GRU to capture the time dependency between time steps. To increase the modeling capacity of BiGRU, we expanded the input dimension of GRU to twice of the mel frequency dimension with full connected networks.

The detailed architecture of ResUNet is shown in Figure 3a. In the downpath, the input low quality mel spectrogram will go through 6 encoder blocks, which includes a stack of L_1 *ResConv* and a 2 by 2 average pooling. In *ResConv*, the outputs of *ConvBlock* and the residual convolution are added together as the output. *ConvBlock* is a typical two layers convolution with BatchNorm and LeakyReLU activation functions. The kernel size of residual convolution and the convolution in *ConvBlock* is 1×1 and 3×3 . Correspondingly, the decoder blocks have the symmetric structure of the encoder blocks. It first performs a transpose convolution with a 2 by 2 stride and 3×3 kernels, which result is concatenate with the output of encoder at the same level to form the input of decoder. The *ConvStack* in decoder also contain L_2 layers of *res-convblock*. The output of the final decoder block is passed to a final *ConvBlock* to fit the output channel.

B.2 SYNTHESIS MODULE DETAILS

As shown in Table 3, we use 7 kinds of STFT resolutions and 4 kinds of time resolution during the calculation of \mathcal{L}_F and \mathcal{L}_T . So $K_F = 7$ in Equation 17 and $K_T = 4$ in Equation 18.

The mel loss \mathcal{L}_{mel} , spectral convergence loss \mathcal{L}_{sc} , STFT magnitude loss \mathcal{L}_{mag} , segment loss \mathcal{L}_{seg} , energy loss $\mathcal{L}_{\text{energy}}$, and phase loss $\mathcal{L}_{\text{phase}}$ are defined in Equation 21, Equation 22, Equation 23,

k	1	2	3	4	5	6	7
win-length	4096	2048	1024	512	256	128	64
hop-length	2048	1024	512	256	128	64	32
fft-size	8192	4096	2048	1024	512	256	128

Table 2: STFT setup for different k in \mathcal{L}_F .

k	1	2	3	4
frame-length	1	240	480	960
hop-length	1	120	240	480

Table 3: Windowing setup for different k in \mathcal{L}_T .

Equation 24, Equation 25, and Equation 26. The function $v(\cdot)$ is the windowing function that divide time sample into w windows and compute mean value within each window, $v(s)_{1 \times w} = (\text{mean}(s_0), \text{mean}(s_1), \dots, \text{mean}(s_{w-1}))$. Each s_w stand for windowed s . Δ stand for first difference.

$$\mathcal{L}_{\text{mel}}(\hat{s}, s) = \left\| \hat{S}_{\text{mel}} - S_{\text{mel}} \right\|_2 \quad (21)$$

$$\mathcal{L}_{\text{sc}}(\hat{s}, s) = \frac{\left\| |\hat{S}| - |S| \right\|_F}{\left\| |\hat{S}| \right\|_F} \quad (22)$$

$$\mathcal{L}_{\text{mag}}(\hat{s}, s) = \left\| \log(|\hat{S}|) - \log(|S|) \right\|_1, \quad (23)$$

$$\mathcal{L}_{\text{seg}}(\hat{s}, s) = \|v(\hat{s}) - v(s)\|_1, \quad (24)$$

$$\mathcal{L}_{\text{energy}}(\hat{s}, s) = \|v(\hat{s}_w^2) - v(s_w^2)\|_1, \quad (25)$$

$$\mathcal{L}_{\text{phase}}(\hat{s}, s) = \left\| \Delta v(\hat{s}_w^2) - \Delta v(s_w^2) \right\|_1, \quad (26)$$

Table 9 and Table 8 show the structure of frequency and time domain discriminators. The sub-band discriminators D_{sub} and multi-resolution time discriminators $D_T^{(r)}(s)$ use the structure of *T-discriminator*, which is a stack of one dimensional convolution with grouping and large kernal size. The frequency discriminator D_F use the similar module *ResConv* similar to *ResUNet* shown in Figure 3b.

T-discriminator
Conv1d(1, 128, kernal_size=16), LeakyRelu(0.2)
Conv1d(128, 128, kernal_size=41, stride=4, padding=20, groups=8), LeakyRelu(0.2)
Conv1d(128, 128, kernal_size=41, stride=4, padding=20, groups=16), LeakyRelu(0.2)
Conv1d(128, 128, kernal_size=41, stride=4, padding=20, groups=32), LeakyRelu(0.2)
Conv1d(128, 1, kernal_size=3, stride=1, padding=1), LeakyRelu(0.2)

Figure 8: The structure of *T-discriminator*.

F-discriminator
Conv2d(1,32,kernal_size=(3,3))
ResConv(32, 32, stride=1,kernal_size=(3,3))
ResConv(32, 32, stride=1,kernal_size=(3,3))
ResConv(32, 64, stride=2,kernal_size=(3,3))
ResConv(64, 64, stride=1,kernal_size=(3,3))
ResConv(64, 32, stride=2,kernal_size=(3,3))
ResConv(32, 32, stride=1,kernal_size=(3,3))
ResConv(32, 32, stride=2,kernal_size=(3,3))
ResConv(32, 32, stride=1,kernal_size=(3,3))

Figure 9: The structure of *F-discriminator*.

B.3 TRAINING DETAILS

Except for the training of vocoder, all other models use the same training setup. We use Adam optimizer with $\beta_1 = 0.5, \beta_2 = 0.999$ and a 3e-4 learning rate. We treat the first 1000 steps as the warmup phase, during which the learning rate grows linearly from 0 to 3e-4. We decay the learning rate by 0.9 every 400 hours of training data. We perform an evaluation every 200 hours of training data. If we observe three consecutive evaluations with no improvement, we will interrupt the experiment.

For all the STFT and iSTFT, we use hanning windows with a window length of 2048 and a hop length of 441. As all the audio we use is at 44.1 kHz sample rate, the corresponding spectrogram size in this setting will be $T \times 1025$, where T is the dimension of time frames. For mel spectrogram, the dimension of the linear spectrogram is transformed into $T \times 128$.

For the training of synthesis module, we setting up the λ_D to λ_{seg} value in Equation 16, Equation 17, and Equation 18 as $\lambda_D = 4.0, \lambda_{\text{mel}} = 50, \lambda_{\text{sc}} = 5.0, \lambda_{\text{mag}} = 5.0, \lambda_{\text{energy}} = 100.0, \lambda_{\text{phase}} = 100.0$, and $\lambda_{\text{seg}} = 200.0$

C APPENDIX C

C.1 DATASETS PREPARATION

Clean speech CSTR VCTK corpus (Yamagishi et al., 2019) is a multi-speaker english corpus containing 110 speaker with different accents. We split it into a training part VCTK-Train and a testing part VCTK-Test. The version of VCTK we used is 0.92. To follow the data preparation strategy of Lee & Han (2021), only the *mic1* microphone data is used for experiments, and *p280* and *p315* are omitted for the technical issues. For the remaining 108 speakers, the last 8 speakers, *p360,p361,p362,p363,p364,p374,p376,s5* are splitted as test set VCTK-Test. Within the other 100 speakers, *p232* and *p257* are omitted because they are used later in the test set DENOISE, remaining 98 speakers are defined as VCTK-Train. Except for the training of *NuWave*, all the utterance are resampled at 44.1 kHz sample rate. AISHELL-3 is an open source Hi-Fi mandarin speech corpus, containing 88035 utterance with a total duration of 85 hours. HQ-TTS dataset contains 191 hours of clean speech data collected from a serial of dataset (van Niekerk et al., 2017; Sodimana et al., 2018; Guevara-Rukoz et al., 2020) on openslr.org. In Table 4, we include the details of *HQ-TTS*, including the URL and language types of each subset.

Table 4: The components of HQ-TTS dataset.

URL	Languages	URL	Languages
http://www.openslr.org/32/	Afrikaans, Sesotho, Setswana and isiXhosa	http://www.openslr.org/70/	Nigerian English
http://www.openslr.org/37/	Bangladesh Bengali and Indian Bengali	http://www.openslr.org/71/	Chilean Spanish
http://www.openslr.org/41/	Javanese	http://www.openslr.org/72/	Colombian Spanish
http://www.openslr.org/42/	Khmer	http://www.openslr.org/73/	Peruvian Spanish
http://www.openslr.org/43/	Nepali	http://www.openslr.org/74/	Puerto Rico Spanish
http://www.openslr.org/44/	Sundanese	http://www.openslr.org/75/	Venezuelan Spanish
http://www.openslr.org/61/	Spanish	http://www.openslr.org/76/	Basque
http://www.openslr.org/63/	Malayalam	http://www.openslr.org/77/	Galician
http://www.openslr.org/64/	Marathi	http://www.openslr.org/78/	Gujarati
http://www.openslr.org/65/	Tamil	http://www.openslr.org/79/	Kannada
http://www.openslr.org/66/	Telugu	http://www.openslr.org/80/	Gujarati
http://www.openslr.org/69/	Catalan		

Noise Data One of the noise dataset we use come from VCTK-Demand (VD) (Valentini-Botinhao et al., 2017), a widely used corpus for speech denoising and noise-robust TTS training. This dataset contains a training part VD-Train and a testing part VD-Test, in which both contain two noisy set VD-Train-Noisy, VD-Test-Noisy and two clean speech set VD-Train-Clean, VD-Test-Clean. To obtain the noise data from this dataset, we minus each noisy data from VD-Train-Noisy with its corresponding clean part in VD-Train-Clean to get the final training noise dataset VD-Noise. The noise data are all resampled to 44.1 kHz. Another noise dataset we adopt is the TUT urban acoustic scenes 2018 dataset (Mesaros et al., 2018), which is originally used for the acoustic scene classification task of DCASE 2018 Challenge. The dataset contains 89 hours of high-quality recording from 10 acoustic scenes such as airport and shopping mall. The total amount of audio is divided into development DCASE-Dev and evaluation DCASE-Eval parts. Both of them contain audio from all cities and all acoustic scenes.

Room Impulse Response We randomly simulated a collection of Room Impulse Response filters to simulate the 44.1 kHz speech room reverberation using a open source tool⁵. The meters of height, width and length of the room is sampled randomly in a uniform distribution $X \sim \mathcal{U}(1, 12)$. The placement of the microphone is then randomly selected within the room space. For the placement of sound source, we first determined the distance to the microphone, which is randomly sampled in a Gaussian distribution $X \sim \mathcal{N}(\mu, \sigma^2)$, $\mu = 2$, $\sigma = 4$. If the sampled value is negative or greater than five meters, we will sample the distance again until it meets the requirement. After sampling the distance between the microphone and sound source, the placement of the sound source is randomly selected within the sphere centered at the microphone. The RT60 value we choose come from the uniform distribution $X \sim \mathcal{U}(0.05, 1.0)$. For the pickup pattern of the microphone, we randomly choose from omnidirectional and cardioid type. Finally, we simulated 43239 filters, in which we randomly split out 5000 filters as test set RIR-Test and named other 38239 filters as RIR-Train.

⁵https://github.com/sunits/rir_simulator_python

C.2 TRAINING DATA SIMULATION ALGORITHM

We describe this simulation process in Algorithm 1. $\mathbb{S} = \{s^{(0)}, s^{(1)}, \dots, s^{(i)}\}$, $\mathbb{N} = \{n^{(0)}, n^{(1)}, \dots, n^{(i)}\}$, and $\mathbb{R} = \{r(0), r^{(1)}, \dots, r^{(i)}\}$ are the speech dataset, noise dataset, and RIR dataset. We use several helper function to describe this algorithm. `randomFilterType()` is a function that randomly select a type of filter within butterworth, chebyshev, bessel, and ellipic. `Resample(x, o1, u)` is a resampling function that resample the one dimensional signal x from a original samplerate o_1 to the target u samplerate. `buildFilter(t, c, o2)` is a filter design function that return a type t filter with cutoff frequency c and order o_2 . `max()`, `min()`, and `abs()` is the element wise maximum, minimum, and absolute value function. `mean()` calculate the mean value of the input.

We first select a speech utterance s , a segment of noise n and a RIR filter r randomly from the dataset. Then with p_1 probability, we add the reverberate effect using r . And with p_2 probability, we add clipping effect with a clipping ratio η , which is sampled in a uniform distribution $\mathcal{U}(\eta_{low}, \eta_{high})$. To produce low-resolution effect, after determining the filter type t , we randomly sample the cutoff frequency c and order o from the uniform distribution $\mathcal{U}(C_{low}, C_{high})$ and $\mathcal{U}(O_{low}, O_{high})$. Then we perform convolution between x and the type t order o lowpass filter with cutoff frequency c . Finally the filtered data will be resampled twice, one is resample to $c * 2$ samplerate and another is resample back to 44.1 kHz. We also perform the same lowpass filtering to the noise signal randomly. This operation is necessary because, if not, the model will overfit the pattern that the bandwidth of noise signal is always different from speech. In this case, the model will fail to remove noise when the bandwidth of noise and speech are similar. For the simulation of noisy environment, we randomly add the noise n into the speech signal x using a random snr $s \sim \mathcal{U}(S_{low}, S_{high})$. To fit the model with all energy level, we randomly conduct a $q \sim \mathcal{U}(Q_{low}, Q_{high})$ scaling to the input and target data pair.

In our work, we choose the following parameters to perform this algorithm, $p_1 = 0.25$, $p_2 = 0.25$, $p_3 = 0.5$, $\eta_{low} = 0.06$, $\eta_{high} = 0.9$, $C_{low} = 750$, $C_{high} = 22050$, $O_{low} = 2$, $O_{high} = 10$, $S_{low} = -5$, $S_{high} = 40$, $Q_{low} = 0.3$, $Q_{high} = 1.0$.

Algorithm 1: Add high quality speech x with random distortions

In: $s \leftarrow \mathbb{S}; n \leftarrow \mathbb{N}; r \leftarrow \mathbb{R}$

$x = s$

with p_1 probability:
 $x = s * r;$ /* Convolute with RIR filter */

with p_2 probability:
 $\theta \sim \mathcal{U}(\Theta_{low}, \Theta_{high});$ /* Choose clipping ratio */
 $x = \max(\min(x, \theta), -\theta);$ /* Hard clipping */

with p_3 probability:
 $t = \text{randomFilterType}();$
 $c \sim \mathcal{U}(C_{low}, C_{high}); o \sim \mathcal{U}(O_{low}, O_{high});;$ /* Random cutoff and order */
 $x = x * \text{buildFilter}(t, c, o);$ /* Low pass filtering */
 $x = \text{Resample}(\text{Resample}(x, 44100, c * 2), c * 2, 44100);$ /* Resample */

with p_4 probability:
 $n = n * \text{buildFilter}(t, c, o);$ /* Low pass filtering on noise */
 $n = \text{Resample}(\text{Resample}(n, c * 2), 44100);$ /* Resample */

with p_5 probability:
 $s \sim \mathcal{U}(S_{low}, S_{high}); q \sim \mathcal{U}(Q_{low}, Q_{high});$ /* Random SNR and scale */
 $n = \frac{n}{\text{mean}(\text{abs}(n)) / \text{mean}(\text{abs}(x))};$ /* Normalize the energy of noise */
 $x = (x + \frac{n}{10^{s/20}});$ /* Add noise */
 $x = qx;$ /* Scaling */
 $x = qx;$ /* Scaling */

Out: The high quality speech s and the randomly distorted version x .

C.3 TEST SET SIMULATIONS

Testing data is crucial for the evaluation on each kind of distortion. The testing data we use either come from publicly available test set or simulated by ourself.

Super-resolution The simulation of SR test set follows the work of (Kuleshov et al., 2017; Wang & Wang, 2021; Lim et al., 2018). The low-resolution and target data pair is obtained by transform 44.1 kHz sample rate utterances in target speech data VCTK-Test to a lower sample rate u . To achieve that, we first convolve the speech data with a order 8 Chebyshev type I lowpass filter with the $\frac{u}{2}$ cutoff frequency. Then we subsample the signal to u sample rate using polyphase filtering. In this work, to test the performance on different sampling rate settings, u are set at 2 kHz, 4 kHz, 8 kHz, 16 kHz and 24 kHz. We denote the corresponding five testing set as VCTK-4k, VCTK-4k, VCTK-8k, VCTK-16k, and VCTK-24k, respectively.

Denoising For the denoising task, we adopt the open-sourced testint set DENOISE described in C.1. This test set contains 824 utterances from a female speaker and a male speaker. The type of noise data comprises a domestic noise (living room), an office noise (office space), noise in transport scene (bus), and two street noises (open area cafeteria and a public square). The test set is simulated at four SNR levels, which are 17.5 dB, 12.5 dB, 7.5 dB, and 2.5 dB. The original data is sampled at 48 kHz. We downsample it to 44.1 kHz to fit our experiments.

Dereverberation The testset for dereverberation, DEREV, is simulated using VCTK-Test and RIR-Test. For each utterance in VCTK-Test, we first randomly select a RIR from RIR-Test, then we calculate the convolution between the RIR and utterance to build the reverberate speech. Finally we build 2937 reverberate and target data pair.

Declipping DECLI, the evaluation set for declipping, is also constructed based on VCTK-Test. We perform clipping on VCTK-Test following the equation in Section 2 and choose 0.25,0.1 as the two setups for the clipping ratio. This result in two declipping testset with different levels, each containing 2937 clipped speeches and targets.

Comprehensive evaluation To evaluate the performance on GSR, we simulate a test set ALL-GSR comprising of speech with all kinds of distortion. The clean speeches and noise data used to build ALL-GSR is VCTK-Test and DCASE-EVAL. The simulation procedure of ALL-GSR is almost the same to the training data simulation described in 5.2. In total, 501 three seconds long utterances are simulated in this testset.

MOS Evaluation We select a small portion from the testsets to carry out MOS evaluation for each one. In SR, DECLI, and DEREV, we select 38 utterances out for human ratings. In DENOISE and ALL-GSR, we randomly choose 42 and 51 utterances.

C.4 EVALUATION METRICS

Log-spectral distance LSD is a commonly used metrics on the evaluation of super resolution performance (Kumar et al., 2020; Lee & Han, 2021; Wang & Wang, 2021). For target signal s and output estimate \hat{s} , LSD can be computed as Equation 27, where $S(f, t)$ and $\hat{S}(f, t)$ is the magnitude spectrogram of s and \hat{s} .

$$LSD(s, \hat{s}) = \frac{1}{T} \sum_{t=1}^T \sqrt{\frac{1}{F} \sum_{f=1}^F \log_{10} \left(\frac{S(f, t)^2}{\hat{S}(f, t)^2} \right)^2} \quad (27)$$

Perceptual evaluation of speech quality PESQ is widely used in speech restoration literature as their evaluation metrics (Pascual et al., 2017; Hu et al., 2020). It was originally developed to model the subjective test commonly used in telecommunication. PESQ provides a score ranging from -0.5 to 4.5 and the higher the score, the better quality a speech has. In our work, we used an open-sourced implementation of PESQ to compute these metrics. Since PESQ only works on a 16 kHz sampling rate, we performed a 16 kHz downsampling to the output 44.1k audio before evaluation.

Structural Similarity SSIM (Wang et al., 2004) is a metrics in image super-resolution. It addresses the shortcoming of pixel-level metrics by taking the image texture into account. We match the implementation of SSIM in (Wang et al., 2004) with ours and compute SSIM as Equation 28, where

Table 5: The experiments we performed. The training sets and testing sets we used during training and evaluation. We use check mark and cross to denote whether a model use the framework of *VoiceFixer* and whether it's trained to perform a SSR or GSR. *VF* here stand for *VoiceFixer*.

Name	VoiceFixer	SSR	GSR	TrainSets	TestSets
Unprocessed					DENOISE; DEREV; SR; DECLI; ALL-GSR;
Oracle-Mel					DENOISE; DEREV; SR; DECLI; ALL-GSR;
Vocoder-TFGAN				VCTK-Train; HQ-TTS; AISHELL-3	DENOISE; DEREV; SR; DECLI; ALL-GSR;
Denoise-UNet	✓			VCTK-Train; VD-Noise;	DENOISE; ALL-GSR;
Dereverb-UNet	✓			VCTK-Train; RIR-Train;	DEREV
SR-UNet	✓			VCTK-Train;	SR
Declip-UNet	✓			VCTK-Train;	DECLI
NuWave	✓			VCTK-Train;	SR
SEANet	✓			VCTK-Train;	SR
SSPADE	✓				DECLI
GSR-UNet		✓		VCTK-Train; VD-Noise; RIR-Train;	DENOISE; DEREV; SR; DECLI; ALL-GSR;
VF-DNN	✓	✓		VCTK-Train; VD-Noise; RIR-Train;	DENOISE; DEREV; SR; DECLI; ALL-GSR;
VF-BiGRU	✓	✓		VCTK-Train; VD-Noise; RIR-Train;	DENOISE; DEREV; SR; DECLI; ALL-GSR;
VF-UNet-S	✓	✓		VCTK-Train; VD-Noise; RIR-Train;	DENOISE; DEREV; SR; DECLI; ALL-GSR;
VF-UNet	✓	✓		VCTK-Train; VD-Noise; RIR-Train;	DENOISE; DEREV; SR; DECLI; ALL-GSR;

μ_S and σ_S is the mean and standard deviation of S . $\text{Cov}_{S\hat{S}}$ is the Covariance of S and \hat{S} . $\epsilon_1 = 0.01$ and $\epsilon_2 = 0.02$ are two constant used to avoid zero division. Similarity is measured within the K 7×7 blocks divided from S and \hat{S} .

$$\text{SSIM}(s, \hat{s}) = \sum_{k=1}^K \left(\frac{(2\mu_{S_k}\mu_{\hat{S}_k} + \epsilon_1)(2\text{Cov}_{S_k\hat{S}_k} + \epsilon_2)}{(\mu_{S_k}^2 + \mu_{\hat{S}_k}^2 + \epsilon_1)(\sigma_{S_k}^2 + \sigma_{\hat{S}_k}^2 + \epsilon_2)} \right) \quad (28)$$

Scale-invariant spectrogram to noise ratio SiSPNR is a spectral metrics similar to Scale Invariant Signal to Noise Ratio (SiSNR) (Le Roux et al., 2019). They have the similar idea except SiSPNR is computed on the magnitude spectrogram. Given the target spectrogram S and estimation \hat{S} the computation of SiSPNR can be formulated as

$$\text{SiSPNR} = 10 * \log_{10} \frac{\|\hat{S}_{\text{target}}\|^2}{\|e_{\text{noise}}\|^2} \quad (29)$$

where $\hat{S}_{\text{target}} = \frac{\langle \hat{S}S \rangle S}{\|\hat{S}\|^2}$. The scale invariant is guaranteed by mean normalization of estimated and target spectrogram.

Scale-invariant signal to noise ratio SiSNR is widely used in literature (Le Roux et al., 2019) to compare the energy of a signal to its background noise. A higher SiSNR indicate less discrepancy between the estimation and target.

D APPENDIX D

D.1 EVALUATION RESULTS

D.2 METRICS CALCULATE ON ANALYSIS MODULE

In this section, we report the mel spectrogram restoration score on different testset. They are calculated for the performance evaluation of the analysis stage. We calculate the LSD, SiSPNR, and SSIM value on each test set. The *Unprocessed* column is calculated using the target and unprocessed mel spectrogram. And the *Oracle-Mel* column is calculated between the target spectrogram and itself.

Table 10 shows that on DENOISE, DEREV, and ALL-GSR, all four *VoiceFixer* based models are effective on the restortion of mel spectrogram. Among the four analysis stage models, *UNet* is consistantly better than the other three models.

Table 11 lists the mel restoration performance on different samplerates. We found that although *VF-BiGRU* have less parameter than *VF-UNet*, it still achieved the highest score on average LSD and

Table 6: Evaluation result on speech super resolution test set SR, which contain five kinds of samplerate settings. The metrics is calculated at a target sample rate of 44.1 kHz

TRAININGS SCHEME		REGRESSION BASED MODELS				VOICEFIXER MODELS				OTHERS		
SampleRate Up Ratio	Metrics	GSR-UNet	SR-UNet	NuWave	SEANet	VF-DNN	VF-BiGRU	VF-UNet-S	VF-UNet	Unprocessed	Oracle-Mel	Target
2kHz 22.1	LSD	1.34	1.19	1.41	1.33	1.18	1.08	1.08	1.05	3.13	0.89	/
	SiSPNR	11.03	10.89	9.19	9.78	10.67	11.84	11.65	12.10	9.18	13.65	/
	SSIM	0.75	0.77	0.73	0.72	0.75	0.77	0.78	0.78	0.68	0.85	/
4kHz 11.0	LSD	1.27	1.18	1.35	1.24	1.15	1.03	1.04	1.02	2.97	0.89	/
	SiSPNR	11.48	11.10	9.65	10.58	11.07	12.27	11.98	12.41	9.52	13.65	/
	SSIM	0.77	0.78	0.76	0.72	0.75	0.79	0.79	0.79	0.71	0.85	/
8kHz 5.5	LSD	1.21	1.11	1.24	1.20	1.06	0.99	1.01	0.99	2.70	0.89	/
	SiSPNR	12.07	11.82	10.73	11.11	11.94	12.68	12.34	12.74	9.93	13.65	/
	SSIM	0.81	0.82	0.80	0.74	0.78	0.81	0.81	0.81	0.76	0.85	/
	MOS	3.37	3.34	3.09	3.37	/	/	/	3.40	3.05	3.53	3.63
16kHz 2.8	LSD	1.10	0.99	1.18	1.16	1.01	0.94	0.96	0.94	2.32	0.89	/
	SiSPNR	13.02	13.01	11.54	11.90	12.37	13.14	12.70	13.14	10.08	13.65	/
	SSIM	0.85	0.88	0.81	0.75	0.82	0.82	0.82	0.82	0.83	0.85	/
24kHz 1.8	LSD	0.97	0.91	1.12	1.15	0.93	0.91	0.94	0.92	1.91	0.89	/
	SiSPNR	13.96	13.81	11.63	12.58	13.21	13.38	12.86	13.38	10.40	13.65	/
	SSIM	0.87	0.91	0.81	0.75	0.84	0.83	0.83	0.84	0.89	0.85	/
	MOS	3.56	3.52	3.54	3.65	/	/	/	3.41	3.47	3.44	3.45
Average Score	LSD	1.18	1.07	1.26	1.21	1.07	0.99	1.01	0.98	2.61	0.89	/
	SiSPNR	12.31	12.13	10.55	11.19	11.85	12.66	12.31	12.75	9.82	13.65	/
	SSIM	0.81	0.83	0.79	0.74	0.79	0.80	0.81	0.81	0.77	0.85	/

Table 7: Evaluation result on speech denoising test set DENOISE

Models	SiSNR	PESQ	SiSPNR	MOS
Unprocessed	8.40	1.97	9.78	3.20
Oracle-Mel	-17.52	2.85	12.84	3.64
Target	/	/	/	3.69
SEGAN *	/	2.16	/	/
Wave-U-Net *	/	2.40	/	/
Wiener *	/	2.22	/	/
Weakly Labelled *	/	2.28	/	/
GSR-UNet	16.42	2.82	12.25	3.64
Denoise-UNet	17.58	2.71	11.82	3.63
VF-DNN	/	1.71	10.93	/
VF-BiGRU	/	2.29	11.72	/
VF-UNet-S	/	2.33	11.19	/
VF-UNet	/	2.43	11.71	3.69

Table 8: Evaluation result on speech dereverberation test set DEREV

Models	PESQ	SiSPNR	MOS
Unprocessed	1.99	14.58	2.70
Oracle-Mel	2.36	13.65	3.46
Target	/	/	3.51
GSR-UNet	2.35	14.10	3.32
Dereverb-UNet	2.49	14.99	3.25
VF-DNN	1.41	11.70	/
VF-BiGRU	1.69	13.00	/
VF-UNet-S	1.78	12.80	/
VF-UNet	1.86	13.21	3.52

SiSPNR. This result shows the recurrent structure is more suitable for the mel spectrogram super resolution task when the initial samplerate is high.

D.3 DEMOS

In this sections we provide a number of restoration demos using our proposed *VoiceFixer*. In Figure 12, we provides eight restoration demos using our VF-UNet model. All the demos we show are the audio collected from the internet or recorded by ourselves. In each example, the left hand side is the unprocessed spectrogram and the right hand side is the restored one. After restoration, these seriously distorted speech can be revert to a relatively high quality one.

Table 9: Evaluation result on speech declipping test set DECLI

Clipping Level	0.25				0.10				Average			
	SiSNR	STOI	PESQ	MOS	SiSNR	STOI	PESQ	MOS	SiSNR	STOI	PESQ	MOS
Unprocessed	9.60	0.95	2.38	2.56	4.00	0.89	1.51	2.72	6.80	0.92	1.95	2.64
Oracle-Mel	-19.94	0.81	2.36	3.44	-19.94	0.81	2.36	3.42	-19.94	0.81	2.36	3.43
Target	/	/	/	3.42	/	/	/	3.49	/	/	/	3.46
GSR-UNet	11.01	0.97	3.54	3.38	7.47	0.94	2.89	3.23	9.24	0.95	3.21	3.31
Declip-UNet	12.45	0.99	3.98	3.38	8.43	0.96	3.40	3.38	10.44	0.98	3.69	3.38
SSPADE	17.43	0.98	3.55	3.34	10.31	0.92	2.12	2.63	13.87	0.95	2.84	2.98
VF-DNN	/	0.76	1.72	/	/	0.72	1.48	/	/	0.74	1.60	/
VF-BiGRU	/	0.81	2.09	/	/	0.79	1.82	/	/	0.80	1.95	/
VF-UNet-S	/	0.82	2.13	/	/	0.80	1.85	/	/	0.81	1.99	/
VF-UNet	/	0.82	2.21	3.38	/	0.80	1.93	3.38	/	0.81	2.07	3.38

Table 10: The Performance of Mel Spectrogram Restoration on DENOISE, DEREV, and ALL-GSR testsets

Models	DENOISE			DEREV			ALL-GSR		
	LSD	SiSPNR	SSIM	LSD	SiSPNR	SSIM	LSD	SiSPNR	SSIM
Unprocessed	1.31	-1.41	0.57	0.84	10.02	0.63	1.65	-3.90	0.47
VF-DNN	0.76	7.61	0.69	0.93	8.86	0.59	0.87	6.26	0.58
VF-BiGRU	0.55	10.98	0.79	0.56	12.91	0.75	0.59	10.49	0.70
VF-UNet-S	0.52	10.29	0.82	0.47	13.61	0.82	0.55	11.08	0.75
VF-UNet	0.46	12.27	0.84	0.46	14.89	0.82	0.53	11.36	0.76

Table 11: The performance of mel spectrogram restoration on SR test set

SampleRate Upsampling Ratio	Metrics	MODELS					
		VF-DNN	VF-BiGRU	VF-UNet-S	VF-UNet	Unprocessed	Oracle-Mel
2kHz 22.1	LSD	0.80	0.68	0.65	0.60	2.99	0.00
	SiSPNR	8.02	9.62	9.82	11.32	2.54	127.43
	SSIM	0.56	0.63	0.66	0.68	0.40	1.00
4kHz 11.0	LSD	0.68	0.54	0.55	0.50	2.54	0.00
	SiSPNR	9.66	12.23	11.22	12.83	3.16	127.43
	SSIM	0.65	0.72	0.74	0.76	0.51	1.00
8kHz 5.5	LSD	0.51	0.40	0.46	0.42	2.02	0.00
	SiSPNR	12.53	14.85	12.67	14.20	4.26	127.43
	SSIM	0.77	0.82	0.83	0.84	0.64	1.00
16kHz 2.8	LSD	0.43	0.26	0.37	0.33	1.53	0.00
	SiSPNR	13.62	19.00	14.07	16.13	5.64	127.43
	SSIM	0.83	0.91	0.90	0.91	0.77	1.00
24kHz 1.8	LSD	0.29	0.18	0.31	0.27	1.16	0.00
	SiSPNR	17.94	22.16	15.53	18.59	7.40	127.43
	SSIM	0.92	0.95	0.94	0.95	0.86	1.00
Average	LSD	0.54	0.41	0.47	0.43	2.05	0.00
	SiSPNR	12.35	15.57	12.66	14.61	4.60	127.43
	SSIM	0.75	0.80	0.81	0.83	0.64	1.00

Figure 12b is the speech I recorded by myself using *Adobe Audition*. I set the sample rate of the original recording to 8 kHz and manually add the clipping effect after recording. It also contains some low-frequency noise and reverberation introduced by the recording device and environment. Figure 12a is a speech⁶ delivered by *Amelia Earhart*, 1897-1937, appeared in the Library of Congress, United States. It's originally a six minutes audio, in which we only select part of them for this demo. The original version sounds like a mumble because it is in low-resolution. Figure 12f is an interview in a TV news program, which includes distortions like room reverberation, noise, and low-resolution. Figure 12e is the audio uploaded by a Youtuber. Probably due to the recording device, her speech is deteriorated seriously by noise and the energy of speech in the low-frequency part is also relatively low. Figure 12c is the restoration of a Chinese famous old movie *railroad guerrilla*. Its speech only has limited bandwidth, and part of the frequency information is completely lost. The audio in Figure 12d is selected from a well-known TV series in China, *romance of the three kingdoms*. It's worth noticing that in the original spectrogram, some parts are masked off due to the audio compression. Figure 12g is a recording selected from a speech delivered by *Sun Yat-sen*, 1866-1925. The speech is in extremely low-resolution and includes multiple kinds of unknown distortions. Figure 12h shows the result of a subway broadcasting I recorded in Shanghai. The low-frequency part of speech almost lost completely and the reverberation is serious.

To sum up, all these examples prove the effectiveness of the *VoiceFixer* model on GSR. And to our surprise, it can generate will on unseen distortions such as the spectrogram lost in Figure 12c, Figure 12f, and Figure 12d. Also, Figure 12e shows that *VoiceFixer* is effective for the compensation of low-frequency energy, making speech sound less machinery and distant. Last but not least, despite the abnormal harmonic structure in the low-frequency part in Figure 12g, our proposed model can still repair it into a normal distribution, which proves the advantages of utilizing the prior knowledge of vocoder.

⁶<https://www.loc.gov/item/afccal000004/>

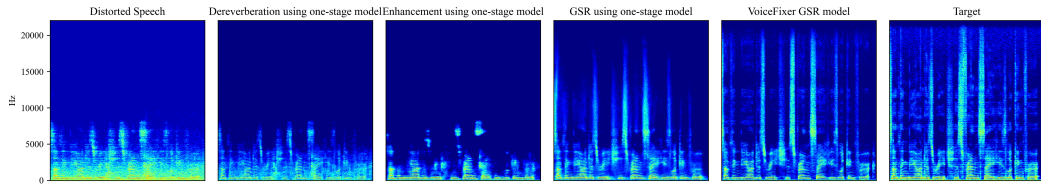
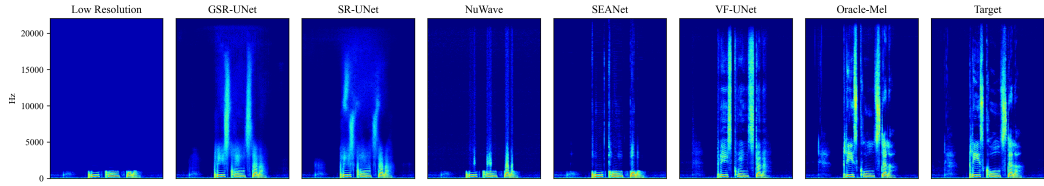
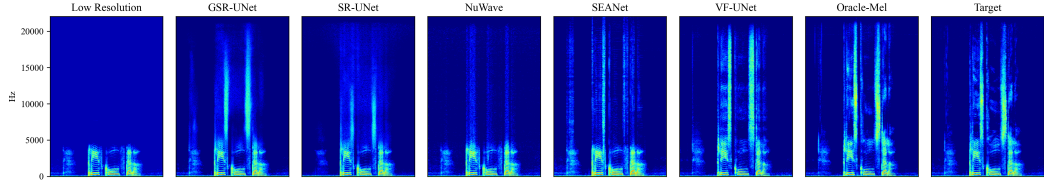


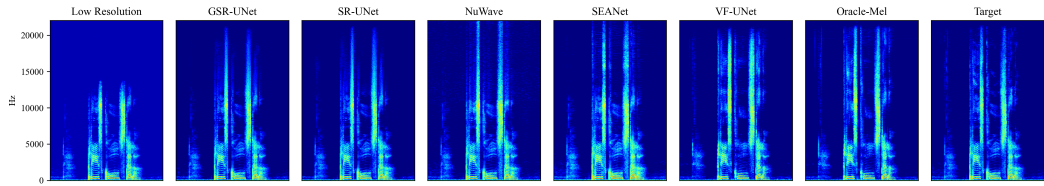
Figure 10: Comparison between different restoration methods. The unprocessed speech is noisy, reverberate and in low-resolution. The leftmost spectrogram is the unprocessed low quality speech and the rightmost figure is the target high quality spectrogram. In the middle from left to right, the figures show results processed by regression based SSR dereverberation model, SSR denoising model, GSR model and *VoiceFixer* based GSR model.



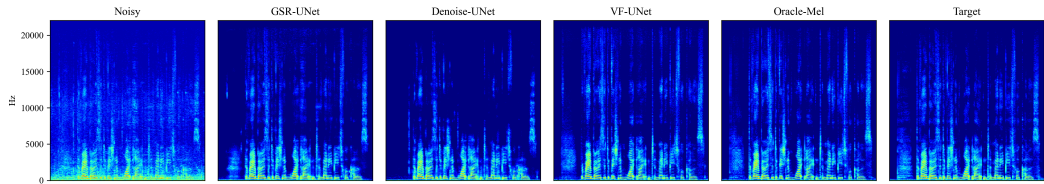
(a) Speech super resolution results on 2 kHz source samplerate test data.



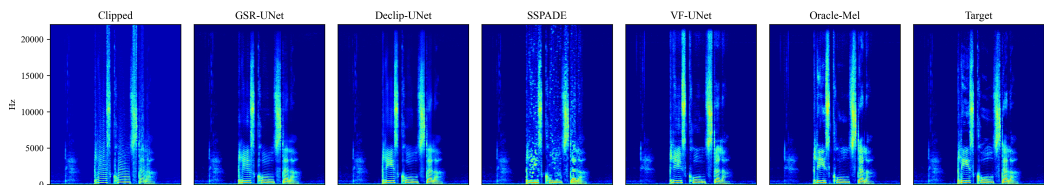
(b) Speech super resolution results on 8 kHz source samplerate test data.



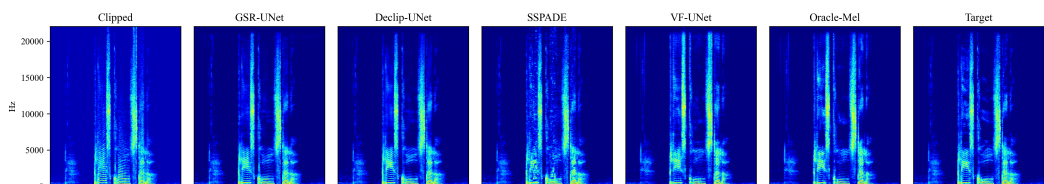
(c) Speech super resolution results on 24 kHz source samplerate test data.



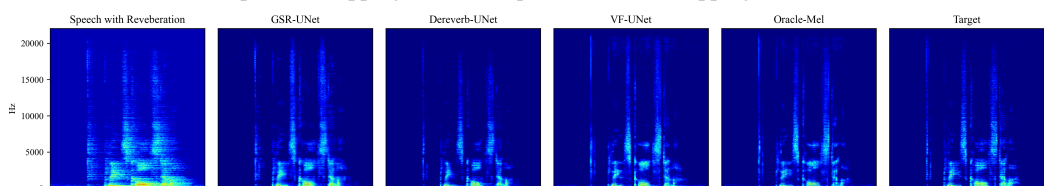
(d) Speech denoising results.



(e) Speech de-clipping results on speech with 0.1 clipping threshold.

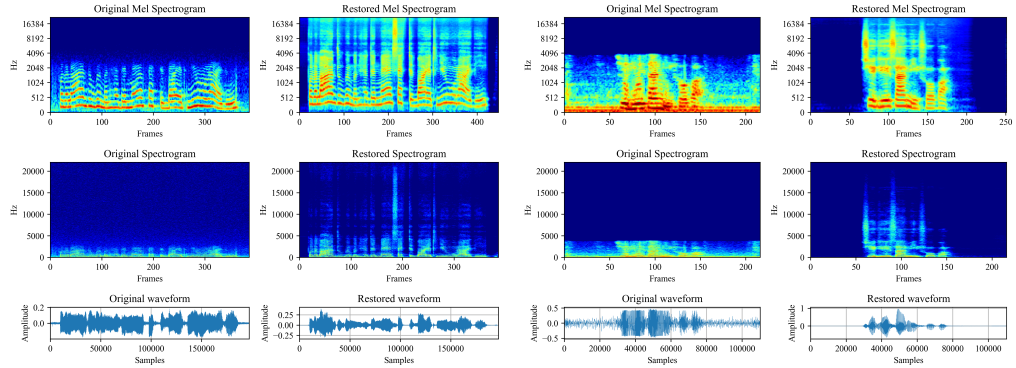


(f) Speech de-clipping results on speech with 0.25 clipping threshold.



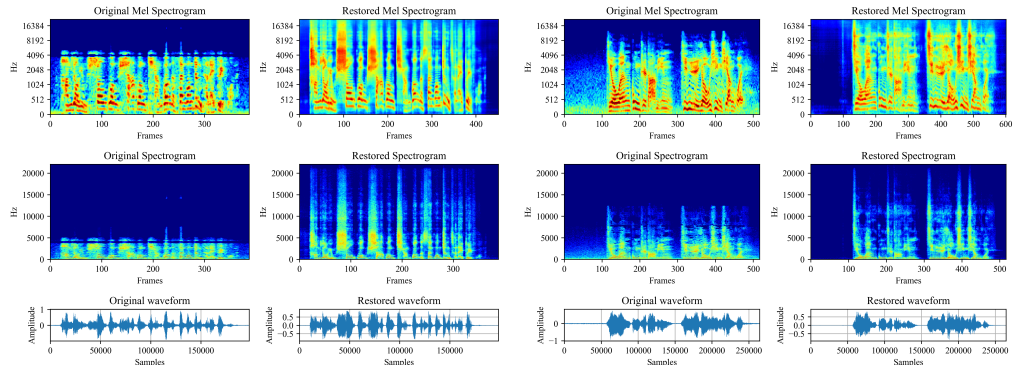
(g) Speech dereverberation results.

Figure 11: Comparison between different model on four different tasks using simulated data.



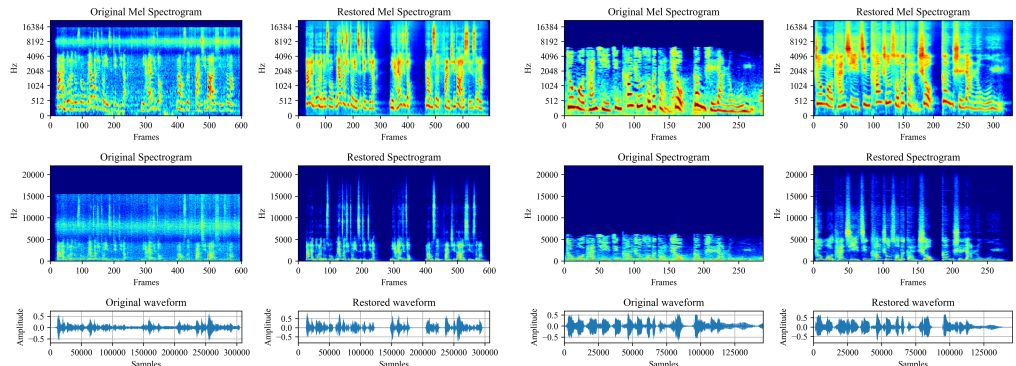
(a) Historical Speech

(b) A Recording Of My Voice



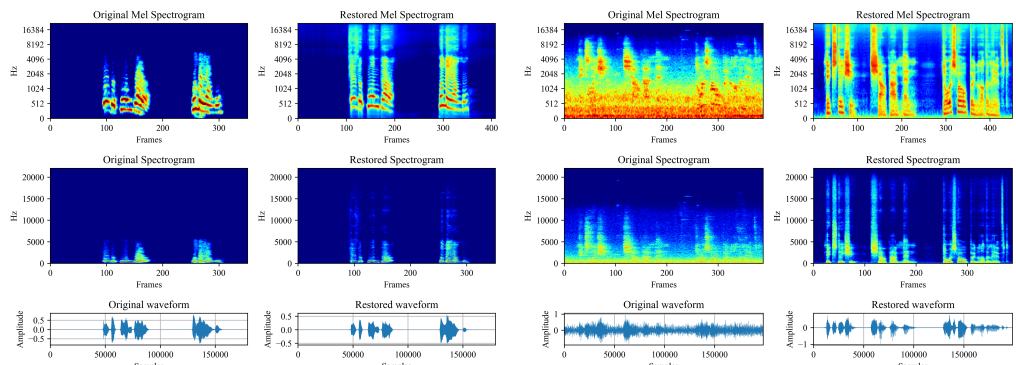
(c) Old Movie

(d) Old TV Series



(e) Chinese Youtuber

(f) Interview in a TV News Program



(g) Historical Speech

(h) Subway Broadcasting

Figure 12: Restoration on the data either collected from the internet or recorded by ourselves.